Diphenyleneiodonium chloride inhibits MYCN-amplified neuroblastoma by targeting MYCN induced mitochondrial alterations

Authors

Soraya Epp[1,9], Stephanie Maher[1,9], Amirah Adlina Abdul Aziz[1,9], Simone Marcone[1], Donagh Egan[1], Saija Haapa-Paananen[2,6], Vidal Fey[2,7], Kristiina Iljin[2,8], Kieran Wynne[1,3], Lasse D. Jensen[4,5], **Walter Kolch[1,3,10], *Melinda Halasz[1,3,10,11]

[1] Systems Biology Ireland, School of Medicine, University College Dublin, Dublin, Ireland

[2] VTT Technical Research Center of Finland., Turku, Finland

[3] Conway Institute of Biomolecular and Biomedical Research, University College Dublin, Ireland

[4] Department of Health, Medicine and Care, Division of Diagnostics and Specialist Medicine, Linköping University, Linköping, Sweden

[5] BioReperia AB, Linköping, Sweden

[6] Present address: FINBB - Finnish Biobank Cooperative, Turku, Finland

[7] Present address: Faculty of Medicine and Health Technology, Tampere University, Tampere, Finland

[8] Present address: VTT Technical Research Centre of Finland Ltd., Espoo, Finland

[9] These authors contributed equally.

[10] Senior author

[11] Lead contact

Correspondence: * melinda.halasz@ucd.ie, ** walter.kolch@ucd.ie

Summary

High-risk neuroblastoma is one of the most lethal childhood cancers. Half of these tumors are driven by MYCN gene amplification (MNA). Despite intensive chemo- and radiotherapy, only 40% of patients survive, and they often suffer from long-term side effects of these genotoxic treatments. Thus, less toxic and more efficacious therapies are needed. Here, we identified diphenyleneiodonium chloride (DPI) as tool compound that preferentially targeted MNA neuroblastoma. Using proteomic and metabolomic assays we investigated the DPI mode of action, finding that DPI could target alterations induced by MNA. These included cell cycle progression, DNA repair pathways, and profound changes in the expression of proteins participating in the mitochondrial electron transport chain. In addition, DPI also downregulated MYCN protein levels preferentially in MNA cells. Metabolic and biological assays suggested that alterations in mitochondrial function and the associated production of reactive oxygen species are critical DPI targets. DPI reduced the proliferation, survival, and malignant transformation of MNA neuroblastoma cells. DPI also shrank tumors and prevented metastatic spread in zebrafish models of neuroblastoma. These findings suggest that processes impacted by DPI could be valuable new targets for the development of non-genotoxic drugs against MNA neuroblastoma.

Keywords

Neuroblastoma, MYCN, mitochondria, zebrafish

Graphical abstract

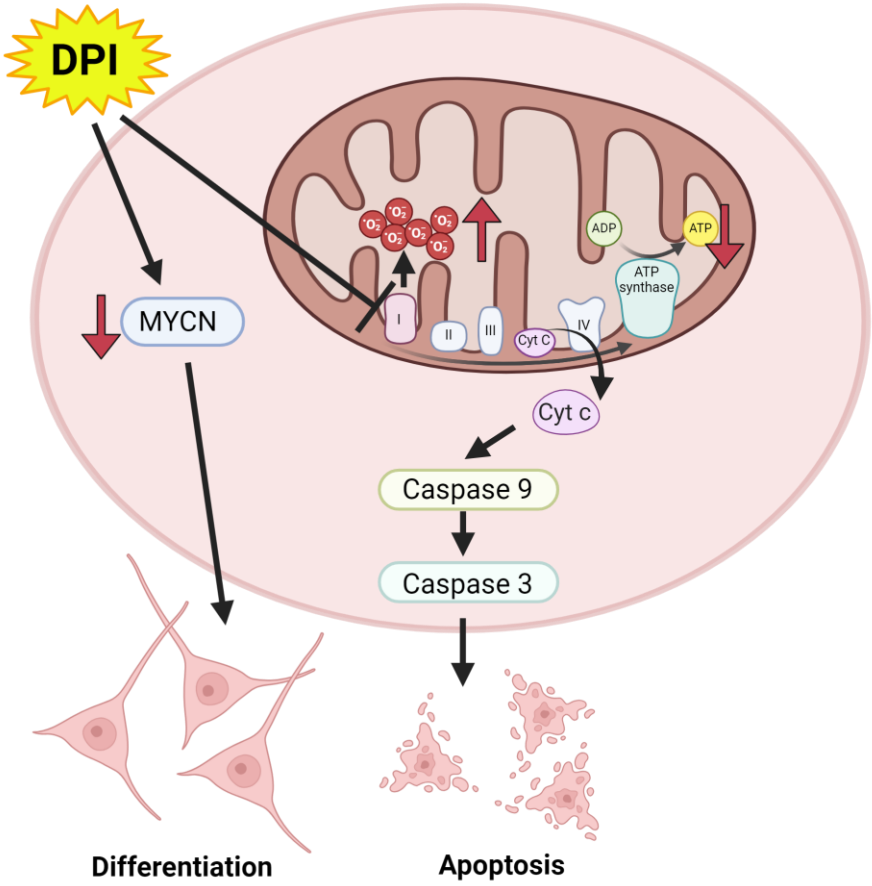

Introduction

Neuroblastoma (NB) is a tumor of the peripheral sympathetic nervous system that accounts for only 6% of childhood cancer cases, but for 15% of deaths from childhood cancers[1]. This disproportionate risk is mainly due to high-risk NB that is driven by amplifications of the MYCN gene. Patients with MYCN amplified (MNA) disease represent about 20% of all patients, and their 5-year event-free survival is only around 40%. They are usually treated with a combination of intensive genotoxic chemotherapy and radiation

therapy. Nevertheless, many patients relapse, leaving them with limited or no treatment options. Furthermore, genotoxic therapies can cause severe long-term toxicities, including cardiovascular problems, hearing loss, secondary cancers, infertility, and endocrine deficiencies[2]. Thus, the current challenge is to identify therapies that are not genotoxic but efficacious. This means that we have to expand the drug target space and find compounds with new modes of action.

The obvious target is MYCN. It is a transcription factor with pleiotropic functions and considered as a master regulator of NB development[3]. However, MYCN is difficult to target directly with drugs, as it lacks apparent pockets where drugs can bind to[4]. Thus, the current main strategies are to block critical MYCN functions and mechanisms that stabilize the inherently unstable MYCN protein[5,6]. However, so far none of these strategies have produced a clinically applicable approach.

Here, we used NB cell lines with regulatable MYCN expression to screen for compounds that preferentially inhibit cells with high MYCN expression. Amongst the most selective compounds targeting high MYCN expressing cells was diphenyleneiodonium chloride (DPI). This compound was originally described as NADPH oxidase inhibitor that reduces the generation of reactive oxygen species (ROS) in the mitochondria, but also has a broader range of targets including NAD/NADP-dependent enzymes in the tricarboxylic acid cycle and pentose phosphate pathway[7]. Newer studies showed that DPI also can induce ROS production by enhancing superoxide production from forward electron transport in complex I of the electron transport chain (ETC)[8]. Malignant cells, including NB cells, often produce more ROS than normal cells, as their increased demand for energy enhances oxidative phosphorylation (OXPHOS) and accompanying ROS production. This mechanism has been identified as a targetable vulnerability of MNA cells[9,10]. Interestingly, MNA NB cells feature an enrichment of

the ROS induced COSMIC mutational signature 18[11], suggesting that ROS contribute to the pathogenetic mechanism of NB.

Investigating the DPI mode of action, we found that DPI targets MYCN dependent alterations in mitochondrial metabolism including OXPHOS and ROS production. Assessing DPI in both in vitro and in zebrafish models of NB showed that DPI could efficiently counteract NB growth and spread.

Results

DPI reduces viability of NB cells and induces cell death in a MYCN-dependent fashion

In order to screen for compounds that preferentially interfere with the viability of MYCN overexpressing NB, we used a SH-SY5Y cell line harboring a doxycycline inducible MYCN transgene (SH-SY5Y/6TR (EU)/pTrex-Dest-30/MYCN cells; called SH-SY5Y/MYCN cells here)[12]. In these cells a 24-hour doxycycline treatment induces a 9fold increase in MYCN protein expression (Fig. S1A). We screened 3,526 compounds (Fig. S1B) measuring cell viability. Using a cutoff of 3-standard deviations of the median, we identified 77 hits that selectively affected the viability of MYCN induced SH-SY5Y/MYCN cells. These hits included compounds that were previously shown to have activity in NB, e.g., gitoxin, a cardenolide glycoside, which inhibits the growth of NB cell lines in mice[13]; inhibitors of MEK, JAK and PI3-kinases, which compromise cell survival[14]; estradiol, which promotes differentiation[12,15]; BH3-mimetics, which induce apoptosis[16,17]; histone deacetylase inhibitors, which are emerging as promising treatments for NB[18-20]; the inosine monophosphate dehydrogenase inhibitor mycophenolate mofetil, which inhibits proliferation and survival of NB cell lines[21]; the Aurora kinase inhibitor AT9283, which was tested in phase 1 clinical NB trials[22]; and inhibitors of DNA methylation (decitabine and 5-azacytidine), which sensitize NB cells to chemotherapeutics[23].

One compound, diphenyleneiodonium chloride (DPI), was more potent in cells where MYCN overexpression was induced (Fig. S1C). DPI was previously reported to protect SH-SY5Y cells against ROS induced cell death[24,25], suggesting that DPI may offer a selective treatment of MNA NB. Therefore, we examined DPI in more detail, especially in respect to its selective impact on MNA cells (Fig. 1). DPI had little differential impact on cellular viability as measured by ATP production in MYCN induced and non-induced SH-SY5Y/MYCN cells (Fig. 1A). However, DPI caused significant and dose-dependent cytotoxicity as measured by loss of membrane integrity (Fig. 1B). A time course analysis showed that cytotoxicity occurred as soon as after 24 hours treatment with increasing differences after 48 and 72 hours (Fig. 1C). Consistent results were obtained with IMR-5/75 cells, a MNA cell line where MYCN expression is down-regulatable by inducing an shRNA against MYCN by doxycycline[26]. Doxycycline treatment reduces MYCN protein expression by ca. 50% (Fig. S1D). The high MYCN levels correlated with low EC50, which increased when MYCN expression was reduced (Fig. 1D). Similarly, DPI cytotoxicity was strongly dependent on MYCN expression (Figs. 1E,F). To further test the MYCN dependency of DPI effects, we measured apoptosis in NB cell lines with normal MYCN expression (SH-SY5Y), MYCN overexpression from a non-amplified allele (NBL-S), and MYCN overexpression from an amplified allele (Be(2)-C) (Fig. S1D, Fig. 1G). DPI selectively induced apoptosis in the MNA Be(2)-C cells.

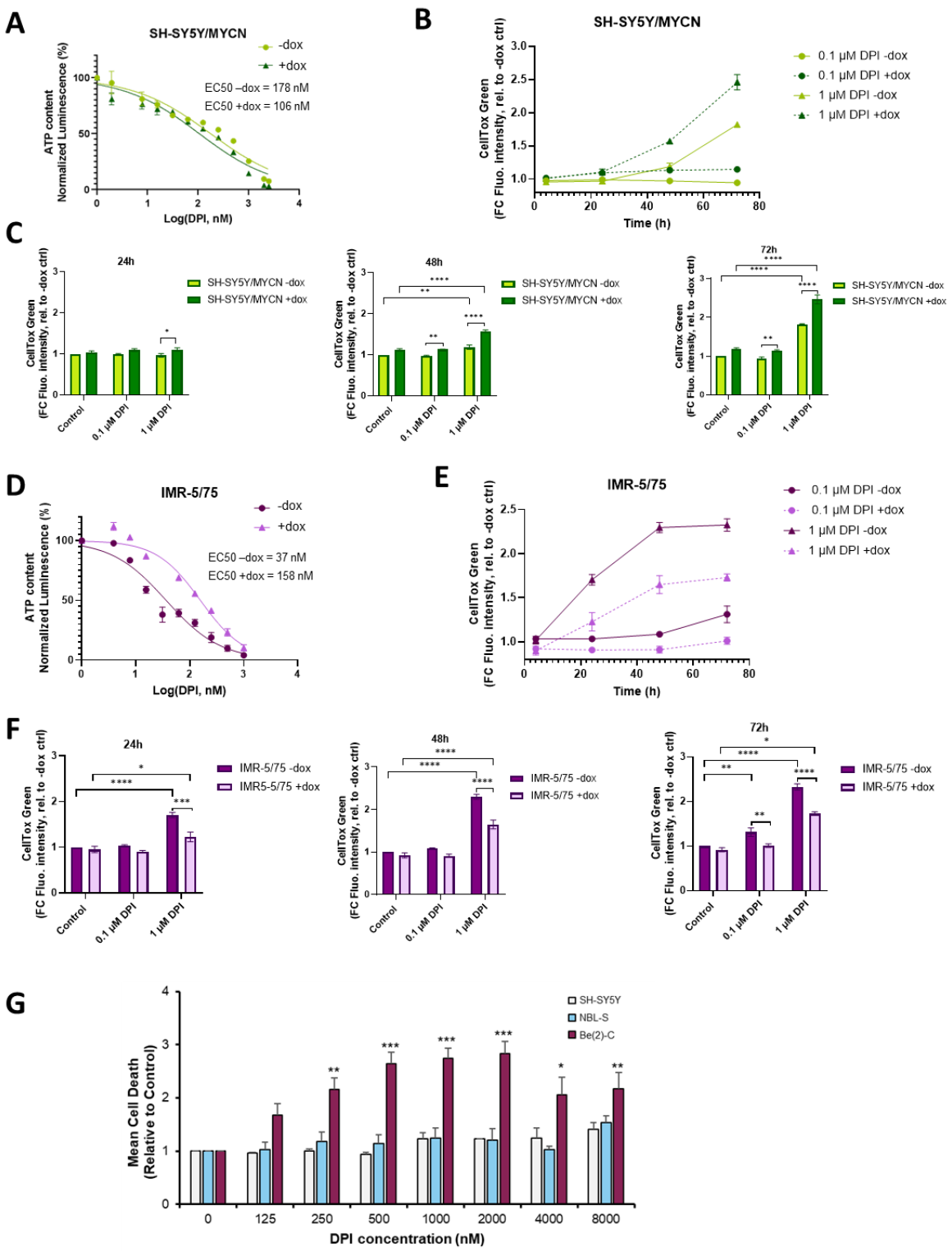

Figure 1. DPI reduces cell viability and induces cell death of NB cells dependent on MYCN levels. **(A)** Cell viability of SH-SY5Y/MYCN cells +/- Dox (1 µg/ml) treated with DPI for 72 hours and assayed by CellTiterGlo. Error bars represent mean ± SEM; N=3. **(B-C)** CellTox Green was used to determine cytotoxicity of DPI in SH-SY5Y/MYCN cells +/- Dox. Error bars represent

mean ± SEM; N=3. Statistical significance was determined by two-way ANOVA, $p<0.05$ = *, $p<0.005$ = **, $p<0.0005$ = ***, $p<0.0001$ = ****. **(D)** Cell viability of IMR-5/75 cells +/- Dox (1 µg/ml) treated with DPI for 72 hours and assayed by CellTiterGlo. Error bars represent mean ± SEM; N=3. **(E-F)** CellTox Green was used to determine cytotoxicity of DPI in IMR-5/75 cells +/- Dox. Error bars represent mean ± SEM; N=3. Statistical significance was determined by two-way ANOVA, $p<0.05$ = *, $p<0.005$ = **, $p<0.0005$ = ***, $p<0.0001$ = ****. **(G)** Apoptosis of the indicated cells was measured by determining the sub-G0/G1 DNA content after treatment with various concentrations of DPI for 72 hours. (Mean± SEM; N=3; $p < 0.05$ = *, $p < 0.001$ = **, $p < 0.0001$ = ***)

Proteomics analysis of DPI-treated Be(2)-C cells

To explore the mechanism of action of DPI, the MNA Be(2)-C cells were treated with DPI (1 h and 24 h), and mass-spectrometry based protein expression profiling and phosphoproteomics were performed. DPI profoundly altered protein expression. Of the 5,048 quantifiable proteins 3,021 (60%) proteins were differentially expressed following DPI treatment (Fig. 2A). Principal component analysis (PCA) showed a clear separation of the three conditions (Fig. 2B). After 1 hour DPI treatment, 213 proteins were upregulated, and 441 proteins were downregulated threefold or more (Fig. 2C). Functional annotation clustering revealed that regulated proteins have functions related to mitochondria, mRNA processing, cell cycle, and GDP-binding. The latter cluster contains small G-proteins of the ARF, RAB and RAS families involved in vesicle transport and mitogenic signaling. After 24 hours DPI treatment, 257 and 1038 proteins were up- and downregulated, respectively (Fig. 2E). Cell cycle, mitochondria and DNA damage clusters remained the top altered functions. (Fig.2F). MYCN was downregulated after 24 hours treatment while the levels of MAX, a binding partner of MYCN remained unaffected.

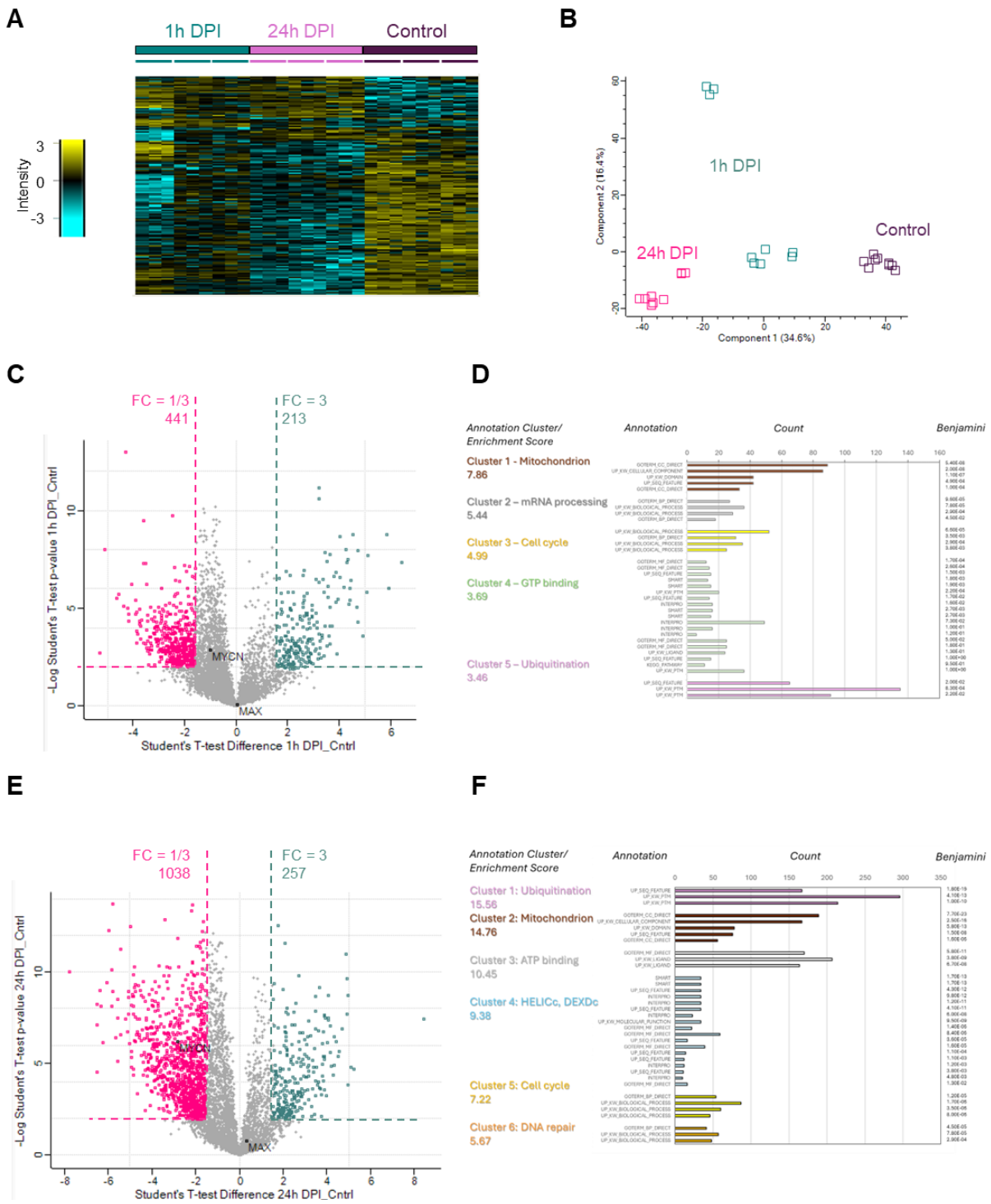

Figure 2. Protein expression profiling of Be(2)-C cells treated with DPI. **(A)** Hierarchical clustering of 3,021 differentially expressed (ANOVA significant) proteins in control and DPI-treated (1 h and 24 h 10 µM DPI) Be(2)-C cells. Each condition has 3 biological and 3 technical replicates. The values in the heatmap represent the Z-transformation of log2(LFQ intensity). Yellow represents high protein expression while blue represents low protein expression. Permutation-based FDR 0.01. **(B)** PCA analysis using a Benjamini-Hochberg FDR = 0.05. **(C)**

Scatter plot, 1h DPI versus untreated control (Ctrl). A 3fold change (FC) was taken as cut-off. **(D)** The top 5 clusters out of 113 clusters following functional annotation clustering of up- and downregulated proteins using DAVID default annotation categories. **(E)** Scatter plot, 24h DPI versus untreated control (Ctrl). A 3fold change (FC) was taken as cut-off. **(F)** The top 6 clusters out of 204 clusters following functional annotation clustering of up- and downregulated proteins using DAVID default annotation categories.

Phosphoproteomics identified 289 differentially regulated phosphorylation sites (Fig. S2A). PCA distinguished the three conditions (Fig. S2B). After one hour DPI treatment, 13 phosphorylation sites were upregulated, and 65 proteins were downregulated threefold or more (Fig. S2C). Functional annotation clustering mapped them to functions related to nucleus, mRNA processing and DNA damage. After 24 hours DPI treatment, 50 and 129 phosphorylation sites were up- and downregulated, respectively (Fig. S2E). Prominently altered functions included ubiquitination, nucleus, cell cycle, and translation initiation. (Fig. S2F).

As the extensive changes in protein expression may influence the quantitation of phosphorylation sites, we integrated protein expression profiling with phosphoproteomics using multifactor analysis[27]. First, we normalized phosphorylation sites against the expression of the respective proteins (Fig. S3A). PCA analysis separated the conditions indicating that changes in both protein expression and phosphorylation independently contribute to the different molecular states induced by DPI treatment (Fig. S3B). The integrated data still discriminated the different treatment conditions revealing the shared sources of variation in the data represented by the factor loadings Z (Fig. 3A). The three conditions are mainly separated by Z1, while variations within conditions are mostly due to Z2. The biological processes and the phosphorylation changes associated with these variations were visualized

by mapping the feature loadings onto pathways and kinases, respectively (Fig. 3B,C). These relationships provide information on the molecular mechanisms that mediate the DPI effects. For example, 1 hour DPI treatment impacts oxidative phosphorylation and Aurora A (AURKA) kinase. Interestingly, in glioblastoma cells AURKA facilitates glycolysis, while suppressing OXPHOS[28]. DPI causes AURKA activation, albeit not significant, (Fig. S3C), which could explain the similar effects of DPI (Fig. 4A). The changes in inositol phosphate metabolism and phosphatidyl-signaling are correlated with increases in the activities of ERK1, KIS, and MAPKAPK3 (MK3) kinases after 24 hours DPI treatment (Fig. S3C). ERK1 and KIS are involved in cell cycle progression, while MK3 promotes cell cycle arrest and senescence[29]. Pathways that characterize untreated control cells include pentose and glucuronate interconversion, which is involved in biosynthetic processes commonly upregulated in cancer[30], and amyotrophic lateral sclerosis, which is hallmarked by dysfunctional mitochondria[31]. Indeed, the corresponding kinases, PAK1, CDK1, and LIMK2 all have been associated with mitochondrial dysfunction[32-34]. Their activities were upregulated by DPI treatment (Fig. S3C). These results strongly suggested that mitochondria contain critical targets for the DPI effects.

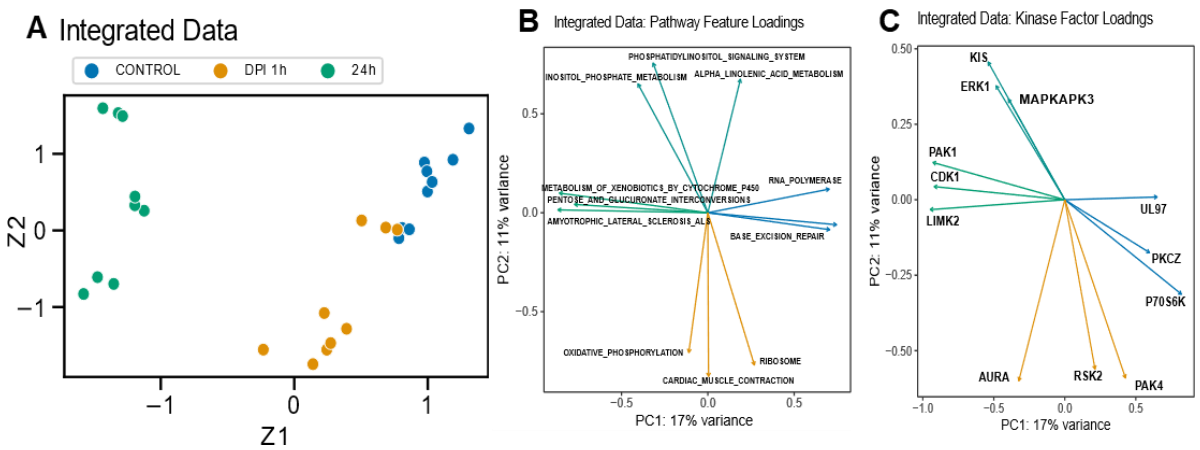

Figure 3. Integration of total proteomics and phosphoproteomics data of DPI-treated Be(2)-C cells by multiset correlation and factor analysis. **(A)** Integration of the whole proteomics

and phosphorylation data. Z1 and Z2 represent shared sources of variation in the data. **(B)** The integrated components (Z1 and Z2) feature loadings indicate which pathways from the protein expression profiling data contribute to the shared sources of variation in the data. **(C)** The kinases from the phosphoproteomics data contributing to the shared sources of variation in the data. Vectors are coloured according to the integrated component they are associated with.

DPI induces mitochondrial superoxide-mediated apoptosis of MNA NB cells

DPI was originally described as NADPH oxidase inhibitor, but in addition to flavin containing enzymes may also inhibit NAD/NADP-dependent enzymes in the pentose phosphate pathway and tricarboxylic acid cycle[7]. DPI also can inhibit complex I in the electron transport chain (ETC) but may selectively enhance superoxide production from forward electron transport enhance while blocking superoxide generation from reverse electron transport[8]. Superoxide dismutase decomposes the highly reactive superoxide to water and hydrogen peroxide which is further detoxified by antioxidant enzymes, such as peroxiredoxins, glutathione peroxidases, and catalases[35].

To measure mitochondrial superoxide production upon DPI treatment we used MitoSOX Red, a dye that selectively detects superoxide. In SH-SY5Y/MYCN cells we did not observe differences in mitochondrial superoxide production upon DPI treatment between doxycycline-induced and non-induced cells (Figs.4A, S4A). By contrast, MNA IMR-5/75 cells produced slightly, but significantly more superoxide in response to DPI, an effect that was abrogated by MYCN downregulation (Figs. 4B, S4B). To examine whether DPI induced superoxide production is linked to MNA, we tested a panel of NB cell lines (Fig. 4C). DPI selectively triggered superoxide production in the MNA cell lines, KCN, KCNR, and Be(2)-C, but not in NBL-S, which overexpress MYCN from a non-amplified allele. DPI induced superoxide to

similar levels as doxorubicin, which is thought to exert cytotoxic effects via superoxide[36].

Inhibited mitochondrial respiration may lead to cytochrome C release from the mitochondrial intermembrane space to the cytosol, leading to activation of caspase-9 and caspase-3 and subsequent apoptosis[37]. DPI caused cytochrome C release in the MYCN-amplified Be(2)-C cells but not in the non-amplified NBL-S cells (Fig. 4D). Cytochrome C release correlated with caspase-9 and caspase-3 cleavage and activation (Fig. 4E). These data suggest that the selective generation of superoxide in the mitochondria of MNA NB cells may be responsible for the preferential efficacy of DPI against MNA NB cells.

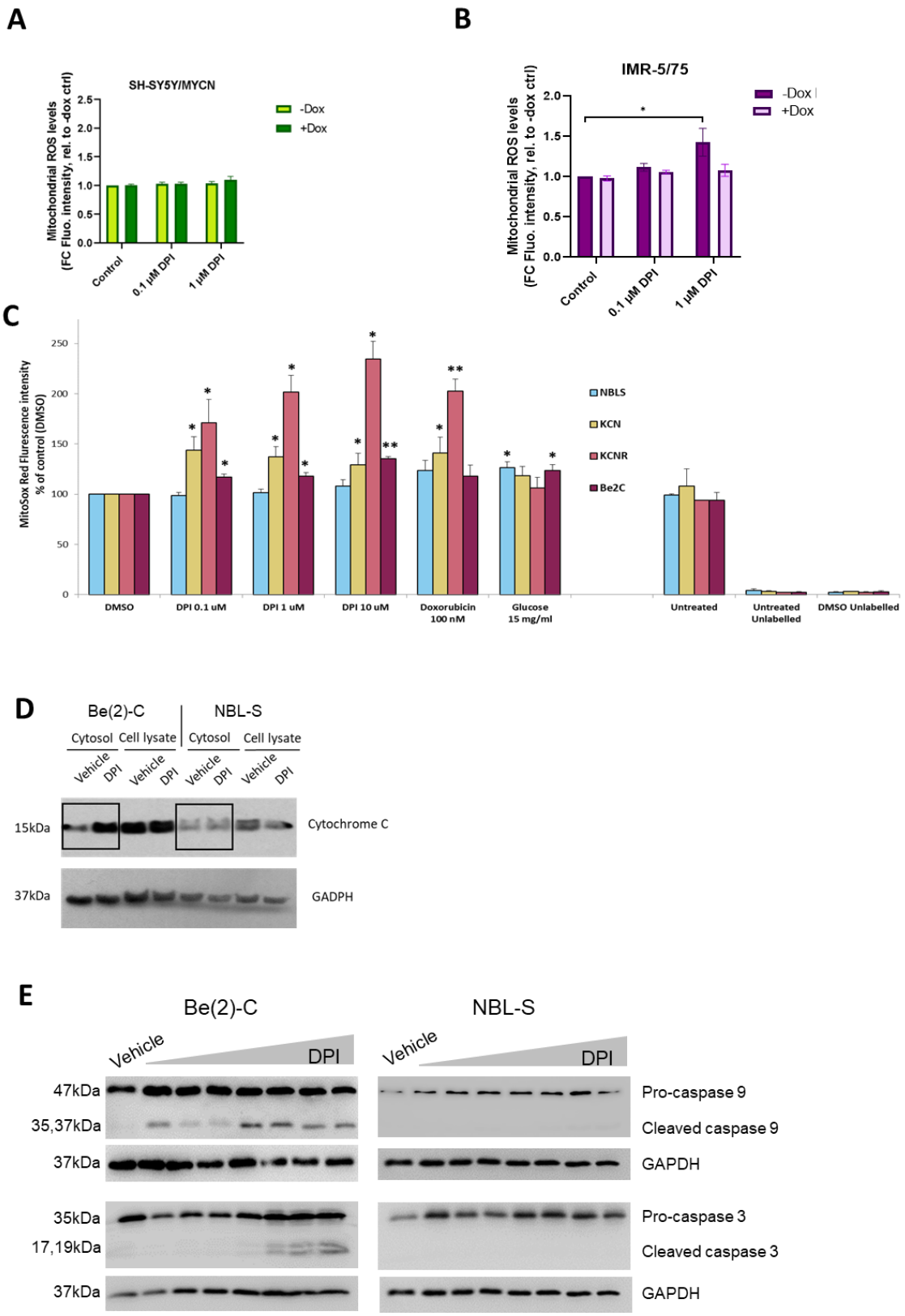

Figure 4. DPI induces mitochondrial superoxide and apoptosis of NB cells dependent on MYCN levels. **(A)** Mitochondrial superoxide production in SH-SY5Y/MYCN +/-Dox treated with DPI for 24 hours detected by MitoSOX-based microscopy. Error bars represent mean± SEM;

N=3; two-way ANOVA, p<0.05 = *, p<0.005 = **, p<0.0005 = ***, p<0.0001 = ****. **(B)** Mitochondrial superoxide production in IMR-5/75 +/-Dox treated with DPI for 24 hours detected by MitoSOX-based microscopy. Error bars represent mean± SEM; N=3; Two-way ANOVA, p<0.05 = *, p<0.005 = **, p<0.0005 = ***, p<0.0001 = ****. **(C)** Mitochondrial superoxide production in DPI-treated NB cell lines detected by MitoSOX-based flow cytometry. NB cell lines were treated with various concentrations of DPI for 24 h. Doxorubicin (100 nM) and glucose (15mg/ml) were used as positive controls. Error bars represent mean± SEM; N=3; $^{**}p < 0.01$, and $^{*}p < 0.05$ treatment vs. DMSO. **(D)** Cytochrome C release was analysed by Western blotting of total cell lysate and the cytosolic fraction in NBL-S and Be(2)-C cells treated with 1µM DPI for 24 hours. **(E)** Caspase-3 and caspase-9 activation was measured by Western blotting in NBL-S and Be(2)-C cells following 24 h DPI treatment (125, 250, 500, 1000, 2000, 4000, 8000 nM).

DPI modulates the expression of mitochondrial genes and MYCN

Given that the DPI effects on mitochondrial respiration seemed MYCN dependent and that c-MYC can affect the expression of ETC components[38], we investigated whether DPI could change the composition of ETC complexes. Our proteomics data in Be(2)-C cells showed that DPI treatment alters the expression of proteins participating in all ETC complexes (Fig. 5A). These changes involved proteins encoded by nuclear as well as mitochondrial DNA. In order to test whether DPI also regulated gene expression on the transcriptional level and across different NB cells, we quantified the expression of mitochondrial genes by RT-qPCR in a panel of DPI treated NB cells (Fig. S5). DPI significantly reduced the expression of most genes in MNA cells with high MYCN expression (Fig. S1D). Taken together, these results suggest that high MYCN expression profoundly affects the composition of all ETC complexes, and that DPI partially can reverse these changes.

Interestingly, DPI also downregulated the expression of MYCN mRNA (Fig. S5) and MYCN protein (Fig. 5B). This effect occurred in all NB cell lines tested, but dose response

curves showed that was more pronounced the higher initial MYCN levels were (Fig. 5B). This could contribute to the enhanced sensitivity of MNA NB cells to DPI.

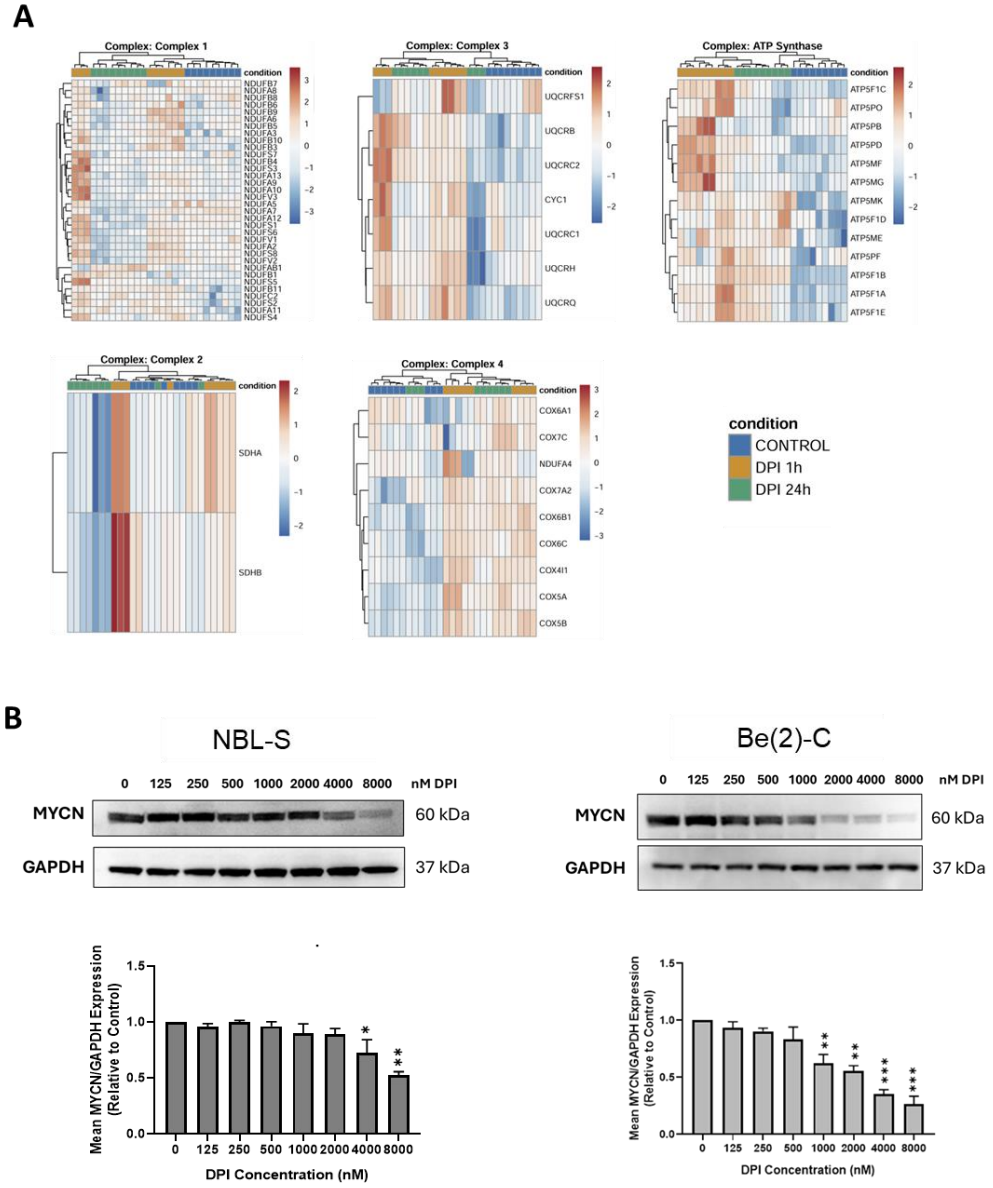

Figure 5. DPI modulates the expression of mitochondrial genes and MYCN. **(A)** Expression changes of proteins contained in mitochondrial ETC complexes as determined by protein expression profiling in Be(2)-C cells. **(B)** Western blot analysis of MYCN protein expression in untreated and DPI-treated (24 h) neuroblastoma cells. Relative MYCN/GAPDH expression compared to the untreated control sample. GAPDH acted as the loading control. Blots were quantitated with Image J, and MYCN expression was normalized to GAPDH. Data is presented as mean +/- SEM of three independent experiments (n=3). P - values were calculated using one-way Anova ($p < 0.05$ = *, < 0.001 = **)

DPI alters mitochondrial metabolism and ATP production

The substantial changes in the expression of ETC complex proteins mediated by MYCN and DPI likely affect mitochondrial functions. Therefore, we measured ATP production in the NB cells with regulatable MYCN by using a SeaHorse Analyzer. ATP can be produced by OXPHOS in the mitochondria or by glycolysis in the cytosol. Total ATP production was higher in IMR-5/75 than in SH-SY5Y/MYCN cells, but DPI reduced it in IMR-5/75 while elevating it in SH-SY5Y/MYCN cells, albeit not significant (Fig. 6A). Interestingly, in IMR-5/75 more ATP (~60%) was produced through OXPHOS than glycolysis, while the ratio was reversed in SH-SY5Y/MYCN cells (Fig. 6B), suggesting that MNA cells are more reliant on ATP generated from OXPHOS compared to non-MNA cells. Regulating MYCN levels only had a small, non-significant impact. By contrast, DPI robustly suppressed mitochondrial ATP production in IMR-5/75 and only non-significantly in SH-SY5Y/MYCN (Fig. 6C). Glycolytic ATP production was significantly enhanced by DPI in both cell lines (Fig. 6D). These results indicate that DPI can push the enhanced mitochondrial ATP production in MNA NB cells back to the levels seen in NB cells with non-amplified MYCN. Taking into account the impact of DPI on the expression of ETC proteins, this normalization may be due to a normalization of the composition of ETC complexes.

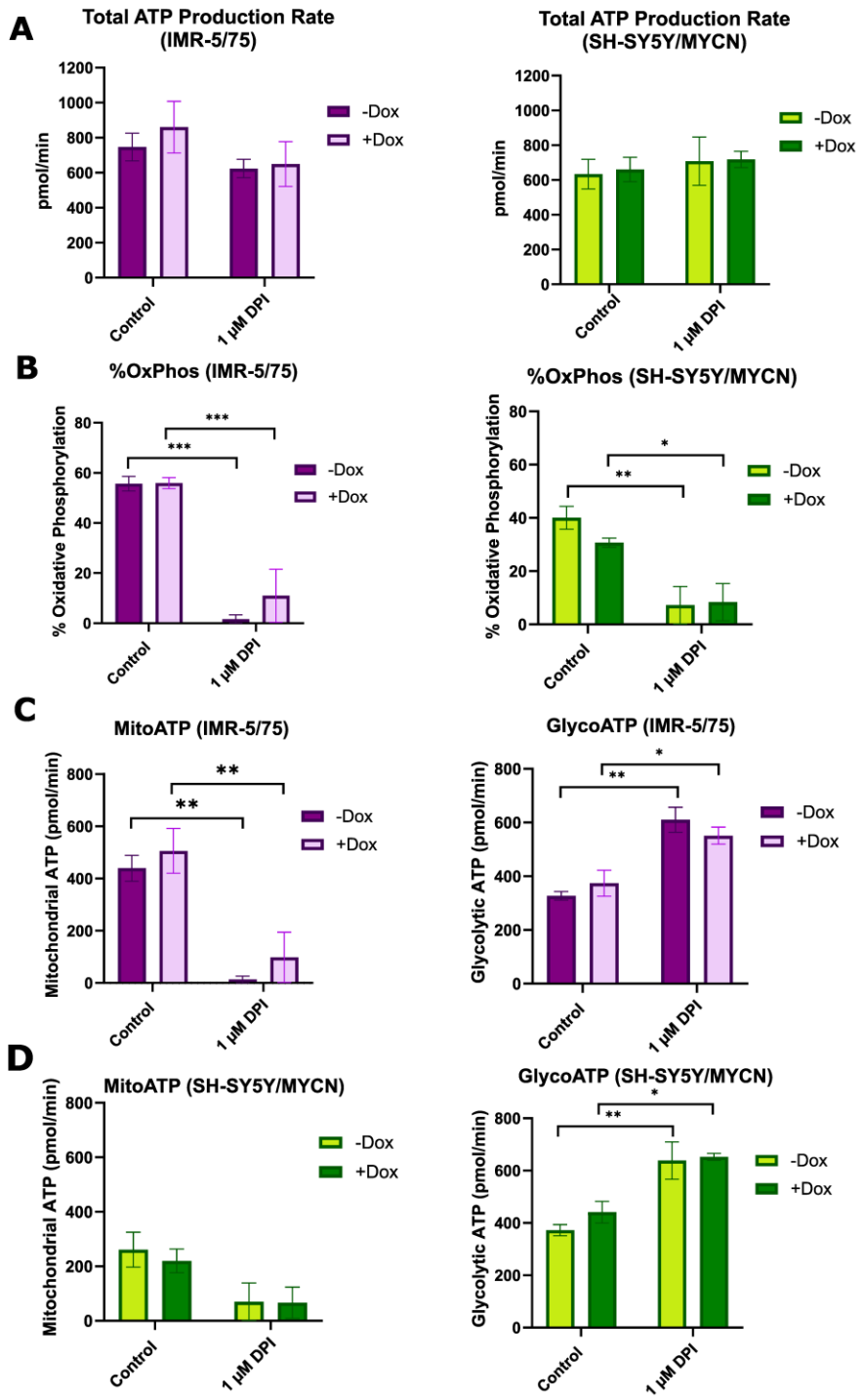

Fig. 6. DPI modulates mitochondrial ATP production. **(A)** Total ATP production from mitochondrial OXPHOS (mito ATP) and cytosolic glycolysis (glyco ATP). **(B)** Percentual OXPHOS contribution to total ATP production. **(C)** ATP produced by OXPHOS. **(D)** ATP produced by glycolysis. Measurements were carried out on cells treated -/+ doxycycline and -/+ DPI (1µM, 24h) using a Seahorse XFe24 Analyzer. Error bars are mean ± SEM; N=3; Two-way ANOVA, $p<0.05$ = *, $p<0.005$ = **, $p<0.0005$ = ***, $p<0.0001$ = ****.

DPI counteracts the malignant phenotype of NB cells

The hallmarks of malignant transformation include resisting cell death and maintaining proliferation at the cost of differentiation[39]. To assess the impact of DPI on these traits we carried out a soft agar colony forming assay and a differentiation experiment. Colony forming assays test the ability of single cells to survive and proliferate into a colony, which are typical properties of cancer cells[40]. The ability to form colonies decreased with lower MYCN expression levels, but DPI completely suppressed colony formation in all NB cells tested (Fig. 7A). Similarly, assessing the potential of cells to undergo neuronal differentiation showed no clear correlation with MYCN expression, but DPI could significantly enhance differentiation in all NB cells tested (Fig. 7B). These results indicate that DPI can counteract both MYCN dependent and independent malignant biological properties of NB cells.

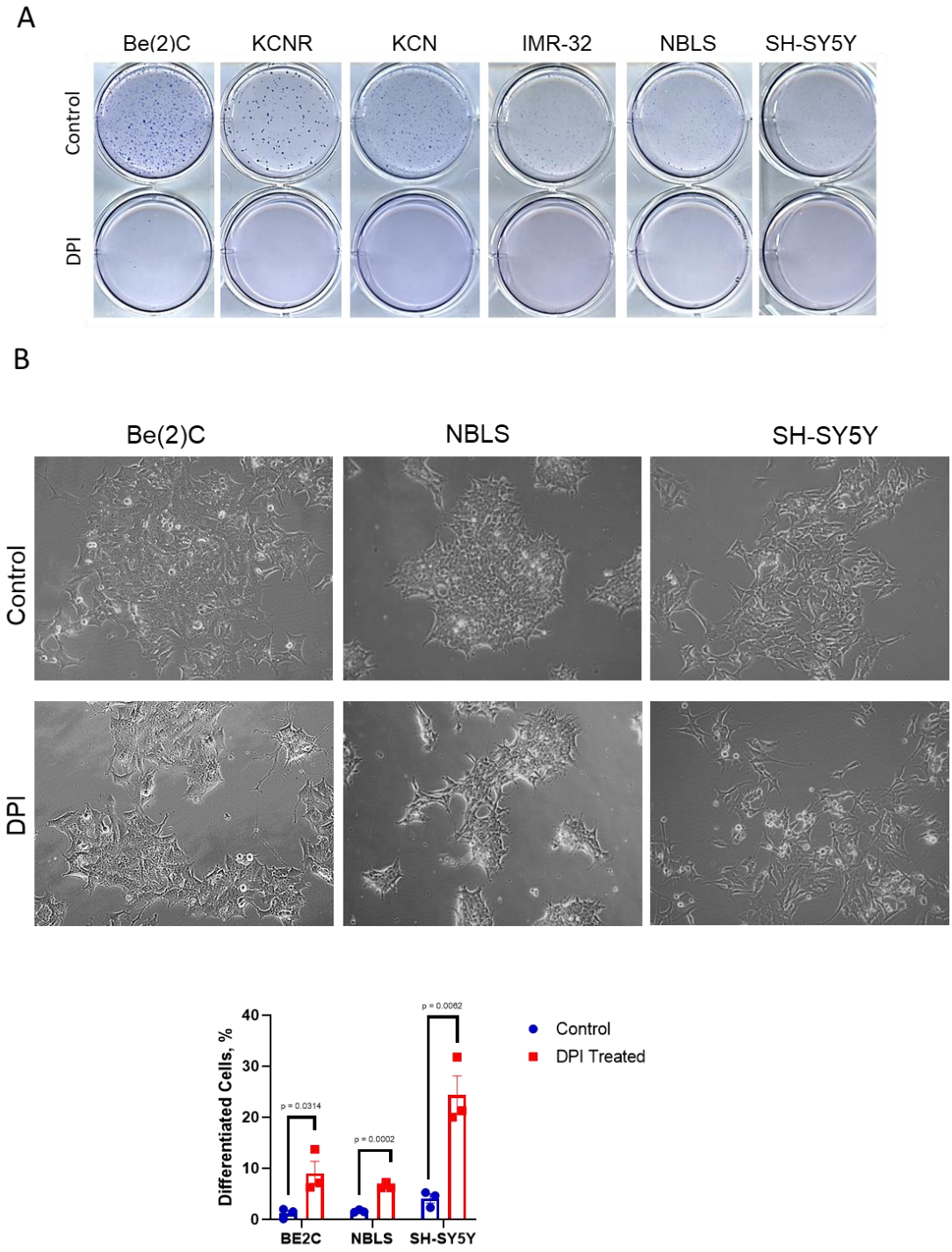

Figure 7. DPI decreases proliferative capacity and induces differentiation of NB cells. **(A)** NB cell lines were subjected to soft agar assay. 10000 cells in 0.48% agarose were layered on a solidified 0.8% base agarose layer per well in 6-well plates. In the presence or absence of 1 µM DPI, plates were monitored for colony formation. Media +/- DPI was replenished every 4 days. After 20 days colonies were stained with crystal violet. **(B)** NB cells were treated with 4 µM DPI or vehicle control for 5 days. Neuronal differentiation was scored by dividing the length

of the longest axon of a cell by the width of the corresponding cell body. Three randomly taken images from 3 independent experiments were examined. Error bars represent mean +/- SEM.

DPI inhibits NB growth and metastatic spread in zebrafish models of NB

To test whether DPI is also active against in vivo tumors, we used a well characterized zebrafish model of MYCN-driven NB. These fish overexpress an EGFP-MYCN transgene in the fish-equivalent of adrenal gland and develop NBs that faithfully recapitulate the genetic and molecular features of human MNA NB[41-45]. Tumors develop spontaneously, and DPI (1 µM) was administered to tumor bearing fish. The treatment was non-toxic and resulted in a significant tumor regression after two weeks of treatment (Fig. 8A). To assess whether tumors formed by human NB cells are also susceptible to DPI, we transplanted fluorescently labelled Be(2)-C cells into the perivitelline space of 2 days old zebrafish embryos and observed them over 72 hours (Fig. 7C-F). The transplants grew and spread throughout the fish. DPI treatment (1 µM) significantly reduced the tumor mass and number of micrometastases in the tail of zebrafish larvae compared to the non-treated group. These findings show that DPI is effective against endogenously arising and transplanted NB suggesting that it could be developed into a non-genotoxic treatment for NB.

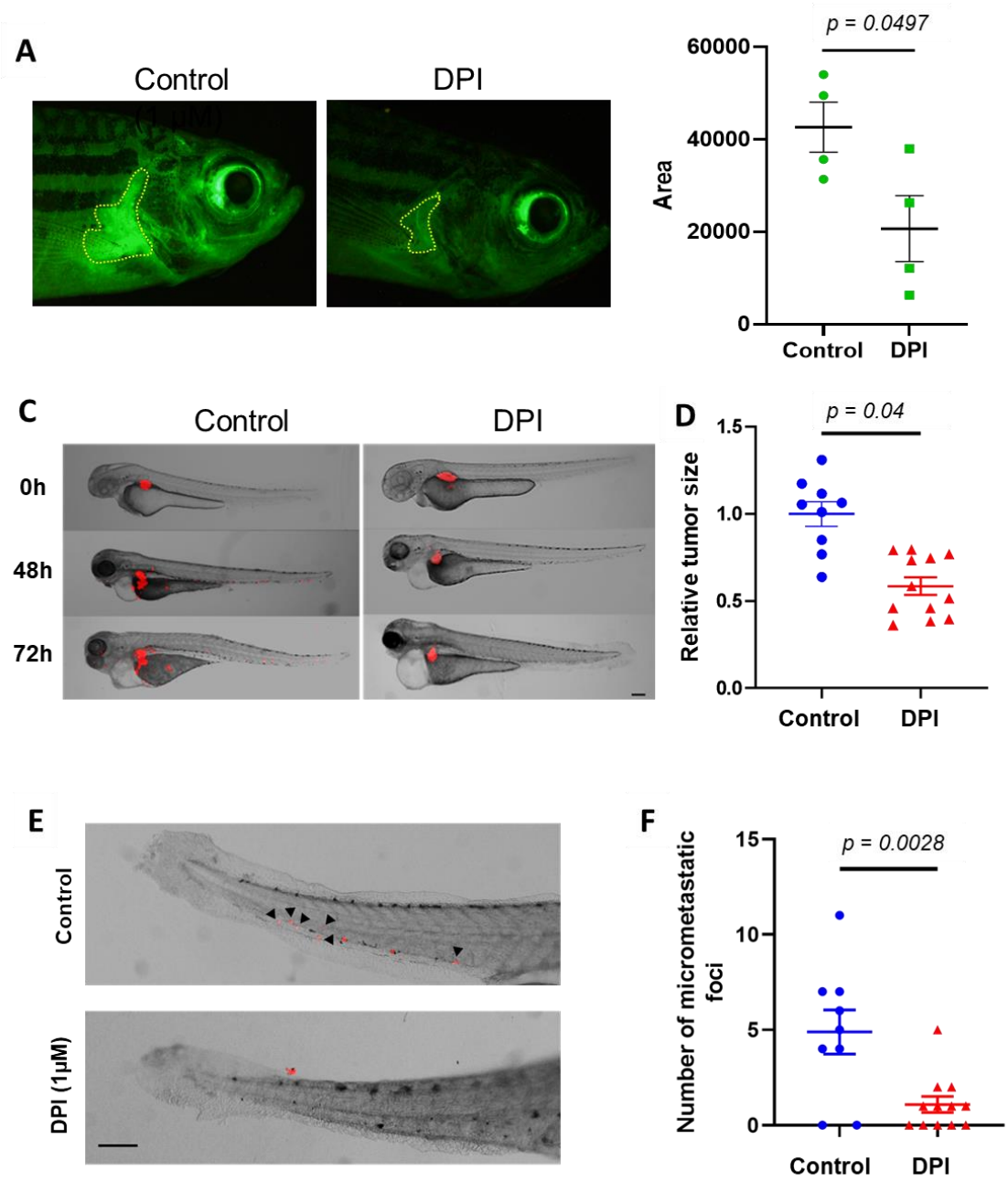

Figure 8. DPI suppresses tumor growth and metastatic spread in zebrafish models of MNA neuroblastoma. **(A,B)** Neuroblastoma growth in a zebrafish model driven by the overexpression of EGFP-MYCN. Tumor bearing fish (15 months of age) were treated with dimethyl sulfoxide (DMSO) control or DPI (1 µM, 14 days). Tumors (marked by broken yellow lines) are easily visualized due to EGFP expression, and their sizes were determined by quantifying green fluorescence. Error bars represent mean ± SEM (two-sample t-test), N = 4. **(C,D)** Be(2)-C cells labeled with red fluorescent dye were injected in the perivitelline space of 2 days post fertilization zebrafish embryos and treated with DPI (1 µM) for 72 hours. Tumor

size was quantified by measuring red fluorescence. Error bars represent mean ± SEM (two-sample t-test). Scalebar is 100 µm. **(E,F)** Black arrowheads indicate micro-metastatic foci in the tail of the fish. Error bars represent mean ± SEM (two-sample t-test). Scalebar is 100 µm.

Discussion

Our results suggest that DPI is a promising tool compound for the development of new non-genotoxic NB treatments. Although we observed no toxicity in our zebrafish experiments, the use of DPI at micromolar concentrations may be limited by toxicity in mammalian species[46]. Therefore, to develop a clinically relevant drug, it is important to understand the mode of action, especially how DPI selectively targets biological processes specific to high-risk NB cells. While DPI was originally discovered as NADPH oxidase inhibitor, it transpired that it affects many more targets[7]. Our findings indicate that most of the relevant DPI actions are related to MYCN overexpression.

While MYCN is clearly a driver gene of high-risk NB, exploiting it as drug target has remined largely elusive[4]. MYCN itself seems not druggable as it has no obvious hydrophobic pockets where small molecule inhibitors can bind. Therefore, indirect approaches have prevailed. For example, Aurora A (AURA) kinase binds to MYCN and protects it from degradation. Aurora A kinase inhibitors (AURAi) destabilize this interaction causing MYCN degradation[47]. They showed promising results in preclinical models but proved ineffective in clinical trials in humans[48]. Recent improvements combined AURAi with ATR kinase inhibitors, exploiting the fact that MYCN activates AURA, and AURA inhibition induces DNA damage that requires ATR kinase for repair[49]. Thus, inhibiting both AURA and ATR prevents MYCN from limiting DNA damage. This mechanism is interesting, as according to our proteomics data DNA repair is an enriched pathway, and DPI treatment reduced the expression of ATR to 29% within 24 hours. Aurora A levels also diminished, albeit to a lesser extent, to 64%. These changes

could plausibly contribute to both the decrease in MYCN protein and the enhanced apoptosis in response to DPI. DPI also modulates the phosphorylation of sites in MYCN that regulate its activation and subsequent degradation, namely T58 and S62[50]. Mitogenic kinases (CDK1, ERK1/2, mTOR) phosphorylate S62 enhancing MYCN activity, while the subsequent phosphorylation of T58 induces S62 dephosphorylation and MYCN degradation. Our normalized phosphoproteomics data show that DPI increases the phosphorylation of MYCN at T58 and S62. In addition, DPI also enhances the phosphorylation of S371 and S375. The corresponding phosphorylation sites in c-MYC, S344 and S348, inhibit both the transcriptional and transforming activity of c-MYC[51]. Thus, DPI may control MYCN activity and stability by multiple mechanisms. Interestingly, the extent of MYCN reduction by DPI correlated with MYCN overexpression suggesting that the suppressive mechanism is under control of MYCN itself. Our previous results showed that MYCN regulates the expression of its own interaction partners[12], and analyzing the impact of DPI on the expression of MYCN interaction partners could provide further insights into how DPI preferentially impacts overexpressed MYCN.

Apart from these effects on MYCN itself, DPI overlaps with MYCN in affecting the function of mitochondria. MYCN overexpression fundamentally changes the metabolic functions of mitochondria[52] and renders MNA cells dependent on MYCN to maintain the function of these altered mitochondria[52]. Our proteomics profiling revealed profound changes in the expression of mitochondrial ETC proteins, which likely would modify the composition and function of ETC complexes. Overexpressed MYCN can increase both glycolysis and OXPHOS[52]. Using Seahorse analysis, we found that MYCN preferentially upregulates OXPHOS. DPI profoundly suppresses OXPHOS while enhancing glycolysis, possibly leading to metabolic imbalance.

As DPI can inhibit ETC complex I in the OXPHOS chain leading to the production of

superoxide[8], the generation of ROS induced by DPI in MNA cells is likely closely related to this metabolic imbalance. DPI was reported to scavenge ROS[24,25], but the altered composition of ETC complexes in MNA cells may subvert this protective function into a deleterious liability. In our experiments the ability of DPI to induce superoxide production, apoptosis, cytotoxicity and decrease of proliferation was linked to MYCN overexpression. The only biological DPI effect that was MYCN independent, was the induction of differentiation. Thus, it seems that the most relevant targets of DPI that suppress MNA NB reside in the mitochondria exerting the metabolic imbalance and superoxide production induced by MYCN overexpression.

Although mitochondria are moving into the limelight as targets for new cancer drugs[53], a wealth of previous experience shows that monotherapies are unlikely to succeed in the clinic. Therefore, DPI will need to be combined with other drugs. Our results suggest that DPI synergizes with chemotherapeutic drugs currently used for NB treatment, such as vincristine, and also with agents that modulate mitochondrial ROS production[54]. Taken together, these data indicate that the MYCN dependent ROS production in mitochondria is the most relevant DPI target for further drug development.

Acknowledgements

This work received funding from Science Foundation Ireland and National Children's Research Centre / Children's Health Ireland through the Precision Oncology Ireland grant 18/SPP/3522, the Science Foundation Ireland Frontiers for the Future Program grant 22/FFP-A/10729, the Irish Research Council grant GOIPG/2020/1361, the Pathological Society of Great Britain and Ireland, Horizon 2020 programme grant H2020-RISE/GA734907 (3D-NEONET), European Union FP7 grant 259348-2 "ASSET," and financial support of Children's Health Foundation under the management of Science Foundation Ireland under the Frontiers for the Future

Programme Grant 21/FFP-P/10130. Mass spectrometry was performed at The Comprehensive Molecular Analytical Platform which was funded by The SFI Research Infrastructure Programme (18/RI/5702). This project was partially supported by the Fight Kids Cancer Funding Programme, supported by Imagine for Margo, Fondation KickCancer, Fondatioun Kriibskrank Kanner, Federazione Italiana Associazoni Genitori e Guariti Oncoematologia Pediatrica and CRIS CANCER Foundation.

Author contributions

Conceptualization, W.K. and M.H.; Investigation, S.E., St.M., A.A., Si.M., S.H.-P., V.F., K.I., K.W., M.H.; Formal Analysis, S.E., St.M., K.I., M.H., D.E.; Writing - all authors contributed to writing the manuscript; Visualization, S.E., D.E., M.H.; Funding Acquisition, W.K., M.H., L.J., St.M., A.A.; Resources, K.I., K.W., L.J.; Supervision, L.J., M.H., and W.K.

Declaration of interests

L.J. is shareholder in BioReperia AB, a company that is developing zebrafish xenograft models for diagnosis and prognosis of cancer patients. The other authors declare no conflicts of interest.

Methods

Cells were generous gifts from J Schulte (Charite, Berlin, Germany) and F Westermann (DKFZ, Heidelberg, Germany). SH-SY5Y and NBLS (single MYCN gene copy) and KCN, KCNR, Be(2)-C (MNA) cells were cultured in RPMI-1640 (Gibco), supplemented with 10% fetal bovine serum (Gibco), 2 mmol/L L-glutamine (Gibco), and 1% penicillin-streptomycin solution (Gibco). For SY5Y/6TR (EU)/pTrex-Dest-30/MYCN cells (here called SH-SY5Y/MYCN cells), where MYCN overexpression is doxycycline inducible[12], the above culture media was supplemented with

Blasticidin (7.5 µg/mL) and G418 (200 µg/mL). For the MYCN-amplified IMR-5/75 cells, where MYCN is downregulatable by doxycycline induction of an shRNA against MYCN[26], the culture media also contained Blasticidin (5µg/mL) and Zeocin(50µg/mL). Doxycycline was used at 1 µg/mL concentration.

Drug screen. SH-SY5Y/MYCN cells were seeded in 384-well plates (1500 cells per well) and treated with 1µg/ml Doxycycline (Sigma) for 24 hours, which resulted in a 11fold increase in MYCN mRNA. Then, uninduced and Doxycycline induced cells were treated with the following drugs: Biomol (80 known kinase and phosphatase inhibitors; at 10, 1, 0.1 and 0.01 µmol/L), LOPAC (1280 compounds; at 1 and 0.1 µmol/L), Microsource Cancer (80 compounds) and Microsource Spectrum (2000 compounds including most of the known drugs and other bioactive compounds and natural products; 1 and 0.1 µmol/L) totaling 3500 compounds (Table 1). Viability was measured 76 hours later using the CellTiter-GLo Luminescence Cell Viability Assay as described previously[12].

Table 1. Compound libraries and concentrations of drugs used for screening

Compound libraries	**Number of compounds**	**Concentrations (mM)**
Sigma LOPAC 1280	1280	0.1, 1
MicroSource Spectrum	2000	0.1, 1
MicroSource cancer plate	80	0.01, 0.1, 1, 10
Biomol International, kinase and phosphatase inhibitors	84	0.01, 0.1, 1, 10
Individually ordered compounds	82	0.1, 1, 10
Total compounds with at least two concentrations	3526	

Western blotting. Cells were lysed with lysis buffer (1% Triton X, 150 mM NaCl, 1 mM $MgCl_2$, and 20 mM Tris–HCl, pH 7.5) supplemented with Complete Mini (Roche) protease and PhosStop (Roche) phosphatase inhibitors. Proteins were resolved in 10% NuPAGE Bis-Tris Mini gels (Life technologies) at 100 V and transferred to a polyvinylidene difluoride membrane (Invitrolon) at 30 V, 70 min. Membranes were blocked using 5% non-fat dried milk (Sigma) in TBS with 0.05% Tween (TBS-T) for 1 h and incubated overnight at 4°C with primary antibodies against MYCN (#sc-53993, Santa Cruz), GADPH (#2118, Cell Signaling), cytochrome C (#Ab110325, Abcam), caspase 3 (#9665, Cell Signaling), or caspase 9 (#9508, Cell Signaling) diluted in 1:1000 in 5% BSA/TBS-T. Membranes were then washed with TBS-T and incubated for 1 h at room temperature with peroxidase conjugated anti-mouse or anti-rabbit IgG (1:5000 dilution, 7076 and 7074, Cell Signaling). Blots were developed using Advanced Molecular Image Imager and ChemoStar Software. Quantification of blots was achieved using ImageJ software v1.44p[55.]

Cell fate assays. Cell viability and cytotoxicity measurements were performed using CellTiterGlo and CellTox Green assays (both from Promega) according to the manufacturer's instructions. Cell death was measured by propidium iodide staining and flow cytometry to identify the fragmented DNA in the sub-G0/G1 population, as previously described[56]. Analysis was performed using an Accuri C6 flow cytometer (BD). For differentiation, cells were observed using light microscopy and images were taken at 10x, 20x, 40x magnification using an Olympus 2-620 camera connected to Olympus CKX41 microscope. Neurite elongation was measured using the NeuronJ Software. Differentiation was scored by dividing the length of the longest neurite by the widest width of the cell body. Cells with neurite length/cell body width

ratios ≥2 were considered differentiated.

For the soft agar assay, 1 ml of 0.8% base agarose layer was placed in each well of 6-well plates, then plates were cooled for 5 min at 4°C to solidify agarose. Then 1 ml of upper agarose layer (0.48%) with 10000 cells was added on the solidified base layer. Then plates were cooled for 5 min, then 1 ml of growth media (+/- 1µM DPI) was added to each well. Plates were incubated at 37°C and 5% CO_2 for 20 days, monitoring for colony formation. Media (+/- DPI) was replaced every 4 days. Colonies were stained by adding PBS containing 4% formaldehyde and 0.005% crystal violet to each well for 1 hour.

Proteomics and phosphoproteomics

Cells were seeded in 15cm^2 dishes in 20 ml culture media. Upon reaching 70-80% confluence, cells were treated with 10 µM DPI for 0, 1 and 24 hours in reverse order, in triplicates. Cells were lysed in ice cold 8M urea/50 mM Tris-HCL pH 8.0, supplemented with phosphatase and protease inhibitors (Roche). Samples were then sonified for 2 X 9 seconds at 10% power using Branson Sonifier® 250 connected to Syclon Ultrasonic Homogenizer. To reduce protein samples, 8 mM dithithreitol (dTT) was added to the samples and incubated in a thermomixer for 60 minutes at 30°C. Then, samples were carboxylated by adding 20 mM iodoacetamide and incubated in a thermomixer for 30 minutes at 30°C in the dark. Samples were diluted in 50mM ammonia bicarbonate. 10 µL of sequencing grade trypsin were added into samples and left overnight on a thermomixer at 37°C to allow sample digestion. The following day, formic acid was added to 1% final concentration to stop sample digestion.

The Glygen TopTipTM C18 protocol (200µL) was utilised for sample clean up. Samples were centrifuged at 5000 rpm for 5 minutes to remove particulates. 200 µL samples were added into a 1.5mL tube and centrifuged at 3000 rpm for 2 minutes. 200 µL equilibration and

washing buffer (0.1% Trifluoroacteic acid (TFA) in high performance liquid chromatography (HPLC) grade water were added and the mixtures were centrifuged at 2500 rpm for 2 minutes. Supernatants were dispensed to waste. 200 µL wetting and elution buffer (80% Acetronitril (ACN) in 0.1% TFA) were added to the pellets and centrifuged at 3000 rpm for 2 minutes. Samples were evaporated for approximately 30 minutes at 30°C in an Eppendorf Concentrator.

TiO2 (titanium dioxide) phosphopeptide enrichment. Dried peptide samples were re-suspended in 500 µL Binding Buffer. TiO2 ratio of beads to sample was weighed out at 10:1. 1 mg of TiO2 was re-suspended in 5 µL of Binding Buffer and mixed on a shaker for 5 minutes at room temperature. 5 µL of TiO2/Binding Buffer was added to each sample. Supernatants were removed and kept in -80°C. TiO2 beads were washed with 1 mL Wash Buffer A (80% Acetonitrile, 1% TFA) and centrifuged at 5000 rpm for 1 minute. Wash Buffer A was then removed, and this step was repeated thrice. Next, TiO2 beads were washed with 1mL Wash Buffer B (80% Acetonitrile, 0.1% TFA) then centrifuged at 5000 rpm for 1 minute. Wash Buffer B was then removed. 50 µL of Elution Buffer (50% Acetonitrile, 25% NH4OH) were added 2 times to elute the "phosphopeptides". Samples were dried for approximately 20 minutes in an Eppendorf Concentrator at 30°C.

LC-MS/MS Method (Bruker timsTof Pro). After trypsin digestion and sample clean up using C18 TT2 TopTips (Glygen), samples were run on a Bruker timsTof Pro mass spectrometer connected to a Bruker nanoElute nano-lc chromatography system. Tryptic peptides were resuspended in 0.1% formic acid. Each sample was loaded onto an Aurora UHPLC column (25cm x 75µm ID, C18, 1.6 µm) (Ionopticks) and separated with an increasing acetonitrile gradient over 90 minutes at a flow rate of 250 nl/min at 45°C.

The mass spectrometer was operated in positive ion mode with a capillary voltage of 1500 V, dry gas flow of 3 l/min and a dry temperature of 180 °C. All data was acquired with

the instrument operating in trapped ion mobility spectrometry (TIMS) mode. Trapped ions were selected for ms/ms using parallel accumulation serial fragmentation (PASEF). A scan range of (100-1700 m/z) was performed at a rate of 10 PASEF MS/MS frames to 1 MS scan with a cycle time of 1.16s.

Data analysis. The raw data was searched against the Homo sapiens subset of the Uniprot Swissprot database (reviewed) using the search engine Maxquant (release 1.6.14.0) using specific parameters for trapped ion mobility spectra data dependent acquisition (TIMS DDA). Each peptide used for protein identification met specific Maxquant parameters, i.e. only peptide scores that corresponded to a false discovery rate (FDR) of 0.01 were accepted from the MaxQuant database search. The normalised protein intensity of each identified protein was used for label free quantitation (LFQ).

Data pre-processing and statistical analysis (multiple sample tests) was performed using Perseus (version 2.1.2.0)[57] for Figs 2 and S2. ANOVA significant proteins were displayed in a heatmap. Selected proteins were further analysed using DAVID[58].

Bioinformatic analysis

The MaxQuant proteinGroups.txt files for both the whole- and phospho-proteomics were filtered to remove known contaminants and protein groups containing no protein. LFQ intensity values were log base 2 transformed, with zero values being assigned NaN to circumvent undefined values. Filtering was applied to keep only those proteins/phosphopeptides with at least 6/9 valid values in at least one drug treatment condition. NaN values were then reassigned to zero before median centering. Site- and condition-specific imputation was performed using the scImpute function in PhosR[59] if the protein was quantified in more than 50% of samples from the same drug treatment. Sample-

wise tail-based imputation was implemented with the tImpute function[59]. Linear regression models were used to determine the relationship between a protein's expression and its phosphorylation levels. The residuals from the linear models were used to normalize the phosphoproteomics data by the whole proteomics data. Differentially abundant phosphosites and proteins between control and DPI-treated samples were identified using the Limma R package. An FDR threshold of 0.05 was used to determine statistical significance.

Multiset correlation and factor analysis. Kinase-substrate relationships were obtained from the PhosphoSitePlus database (https://www.phosphosite.org/homeAction.action), while pathway-gene relationships from the KEGG database were accessed through MSigDB. Both the pathways and kinases were scored in the whole proteomics and phosphoproteomics datasets using the GSVA function in R. The resulting scores, which represent the activity levels of kinases and pathways in each sample, were then used as input for Multiset Correlation and Factor Analysis[27]. This analysis was conducted using default parameters to identify shared factors of variation across both omics' datasets. Kinases and pathways that contributed most to the variation between sample conditions were selected based on their absolute feature loadings.

Cell fractionation. Mitochondria were isolated using the Qproteome Mitochondria Isolation Kit according to manufacturer's instructions (Qiagen). Ten million cells have been used for the isolation of mitochondria and the purity of the fraction was assayed by Western blotting for cytosol (GADPH) or mitochondria (cytochrome C) specific proteins.

MitoSOX Red staining. Mitochondrial superoxide levels were assessed using the MitoSOX Red

fluorescent indicator (Thermo Scientific) by flow cytometry of live cell imaging, according to manufacturer's instructions.

Flow cytometry: $1x10^5$ cells were seeded in a 12 well plate and treated with vehicle (DMSO) or DPI for 24h. After treatment, 1 ml of HBSS buffer with 2.5 µM of MitoSOX™ reagent was added to the cells and incubated for 10 minutes at 37°C. Cells were detached using Versene solution and after two washes in HBBS were re-suspended in 500 ml of HBBS for flow cytometry analysis. Forward and side scatter gates were established to exclude non-viable cells and cell debris from the analysis. Auto-fluorescence signals generated by unlabeled cells were used as negative controls in each experiment. Flow cytometric analysis was performed on an Accuri C6 instrument by using the FL2 detector (Optical Filter 585/40 nm) and analyzed with CFlow® Software (Accuri, Ann Arbor, MI, USA). The data were expressed as median fluorescence intensity of three independent experiments.

For imaging, cells were typically seeded in 100 µL of RPMI phenol red-free media per well in duplicate on a black 96-well plate with a clear bottom (Thermo Scientific). To ensure IMR-5/75 and SH-SY5Y/MYCN cells remained attached, the plates were pre-coated with 100 µg/mL Poly-D-Lysine (Sigma-Aldrich). 24 hours post-doxycycline induction, the cells were treated with 100 µL of DPI or vehicle and incubated at 37°C. Following the designated incubation period, cells were rinsed once with DPBS containing Ca 2+ /Mg 2+ (Invitrogen). MitoSOX Red dye (4 µM) was then added along with the Hoechst 33342 nuclear counterstain (1 µg/mL) (Thermo Scientific) in DPBS containing Ca 2+ /Mg 2+ and incubated for 20 minutes at 37°C, shielded from light. After incubation, cells were washed twice, and fresh RPMI phenol red-free media was added before live-cell imaging. The MitoSOX Red indicator was detected using the TRITC filter (Ex/Em: 396/580 nm) and Texas Red filter (Ex/Em: 560/630 nm), while Hoechst was detected using the HOECHST 33342 filter (Ex/Em: 353/483 nm).

Live cell imaging. Confocal images were captured across four optical planes spaced 1 µm apart (ranging from -1.0 µm to 2.0 µm) within 25 x 25 fields of view, with a 10% overlap per well, using an Opera Phenix High Content Screening System (PerkinElmer). The imaging was performed with either a 40x or 63x/1.15 NA water-immersion objective under live cell conditions (37 °C and 5% CO2). The images obtained were analyzed using an optimized pipeline tailored for each cell line on Harmony® v.4.9 high-content analysis software (PerkinElmer). The software's building blocks were employed to identify and calculate the mean dye parameters per well, including the number of nuclei and MitoSOX Red mean intensity per cell.

qRT-PCR. Total RNA was isolated from NB cell lysates using the RNeasy kit (Qiagen, UK). Reverse transcription was carried out on 1000 ng of total RNA using Superscipt III reverse transcriptase (Invitrogene) according to the manufacturers' instructions. Quantification of gene expression by real-time PCR was performed on an ABI Prism 7700 Sequence Detection System, (Applied Biosystems Inc., UK). MT-ND1, MT-ND2, MT-ND3, MT-ND4L, MT-ND6, MT-ATP6, MT-ATP8, MT-CO1, MT-CYB, TFAM, and MYCN gene expression was examined using specific Taqman gene expression assays (Applied Biosystems Inc., UK). GADPH was used as endogenous control in the assay.

Metabolic measurements. Metabolic activity was evaluated using a Seahorse XF24 Analyzer (Seahorse Biosciences) through an ATP rate test. IMR-5/75 and SH-SY5Y/MYCN cells were seeded at 37,500 cells per well in PDL-coated XF microplates and incubated in XF RPMI medium with glucose, sodium pyruvate, and glutamine. After six hours, doxycycline was

added to induce gene expression in specific wells. On the second day, cells were treated with DPI or vehicle, and the XFe24 Sensor Cartridge was hydrated overnight. On the third day, cells were washed with assay medium, incubated, and the ATP rate test was conducted by sequentially injecting oligomycin A and a mix of rotenone and antimycin A. Post-assay, cells were fixed with glutaraldehyde, stained with Crystal Violet for normalization, and absorbance was measured. Data was analyzed using Wave software to generate key metabolic parameters, including Oxygen Consumption Rate (OCR), Proton Efflux Rate (PER), and Extracellular Acidification Rate (ECAR), followed by statistical analysis in GraphPad Prism.

Zebrafish experiments were approved by the University College Dublin Animal Research Ethics Committee and the Healthcare Products Regulatory Authority (AE18982/P038). zebrafish (Danio rerio) were maintained at 28°C on a 14-hour light/10-hour dark cycle.

Xenografts: At 2dpf, dechorionated zebrafish embryos were microinjected with fluorescently labelled Be(2)-C cells. Prior to microinjection, embryos were transferred to prewarmed 2% agarose gel and anaesthetized with 0.05mg/mL Tricaine. Be(2)-C cells were fluorescently labelled with DiI. Approximately 100-500 cells were injected into the perivitelline space of each embryo. Following injection, embryos were screened and randomly assigned a treatment arm. Each embryo was placed in an individual well of 24 well plate containing 600uL PTU ± DPI (1 uM). Embryos were incubated at 35 °C for duration of treatment (72 h). Embryos were imaged daily using fluorescent microscopy (Nikon Eclipse C1) to monitor tumour progression and metastasis. Data analysis was carried out using ImageJ, Excel and GraphPad Prism.

The Tg[dbh:MYCN-EGFP] transgenic zebrafish was a generous gift from A. T. Look (Dana-Farber Cancer Institute, Harvard Medical School)[44]. Adult Tg[dbh:MYCN-EGFP] zebrafish

were monitored for fluorescent tumor masses biweekly. Zebrafish developing the fish-equivalent of human neuroblastoma in the interrenal gland (age, 15 months; n = 4) were treated every 48 hours with DPI for 2 weeks. Variance in tumor size for all fish at pretreatment was <5%. Zebrafish were anesthetized by 0.016% tricaine before microscopic analysis. An Olympus SZX10 fluorescence stereomicroscope equipped with an Olympus DP71 camera was used to capture images. The fluorescent region posterior to the gills, which corresponds to the region of neuroblastoma growth[44], was analyzed using ImageJ software (version 1.44p).

Supplementary Figures

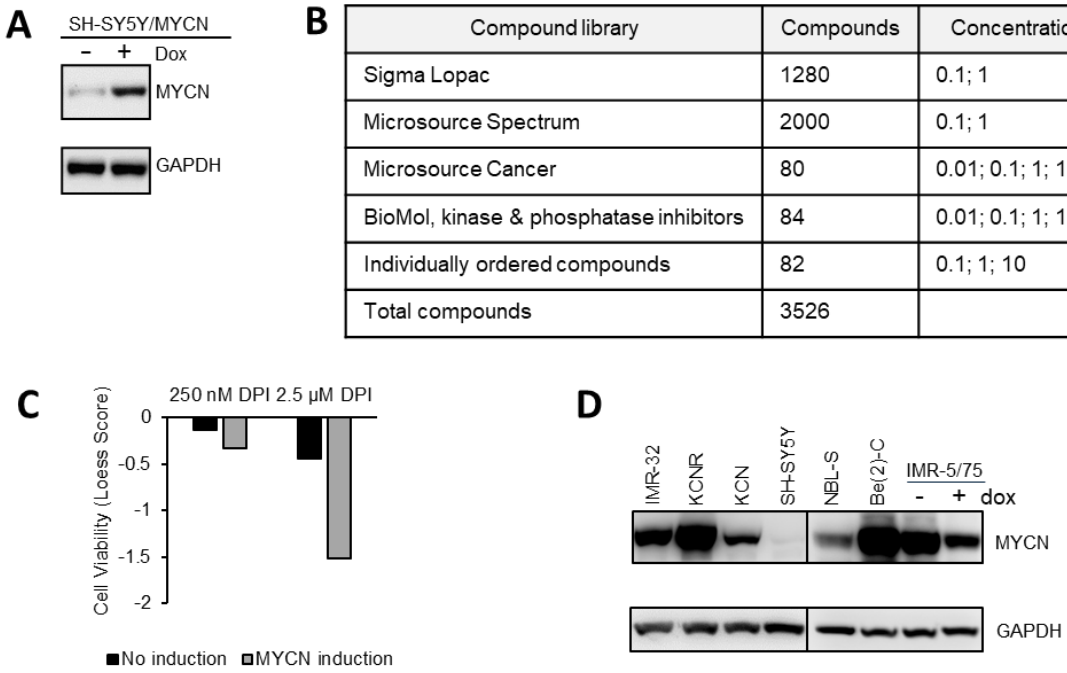

Compound library	Compounds	Concentrations (µM)
Sigma Lopac	1280	0.1; 1
Microsource Spectrum	2000	0.1; 1
Microsource Cancer	80	0.01; 0.1; 1; 10
BioMol, kinase & phosphatase inhibitors	84	0.01; 0.1; 1; 10
Individually ordered compounds	82	0.1; 1; 10
Total compounds	3526	

***Supplementary Figure S1. DPI reduces cell viability and induces cell death of NB cells dependent on MYCN levels*. (A)** MYN protein levels in SH-SY5Y/MYCN cells before and after a 24-hour induction with doxycycline (Dox). **(B)** Compound libraries used for screening. **(C)** Cell viability of DPI treated SH-SY5Y/MYCN cells +/- Dox measured by CellTiterGlo. **(D)** Western blot of MYCN expression in the indicated cell lines.

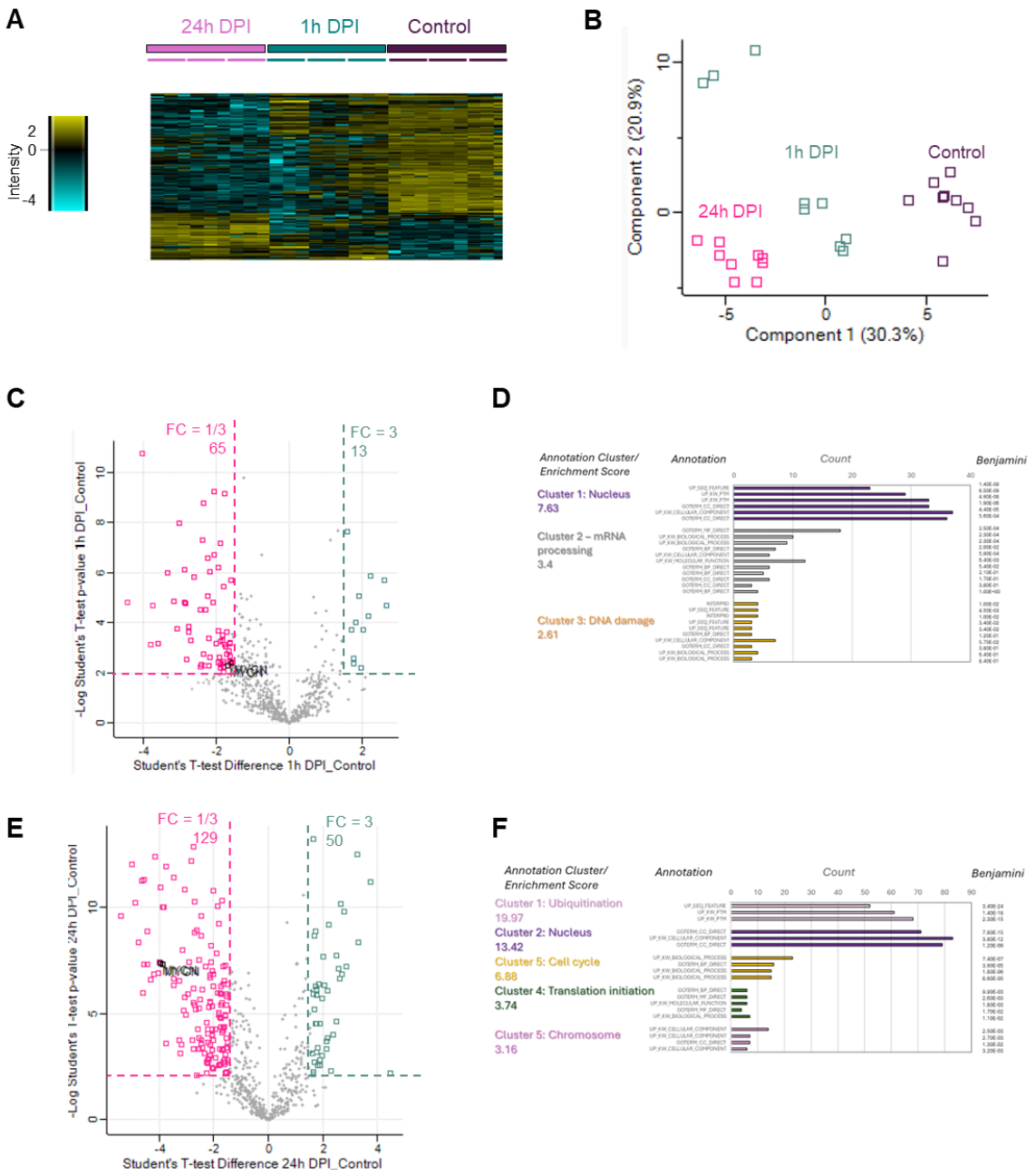

Supplementary Figure S2. Phosphoproteomics of Be(2)-C cells treated with DPI. **(A)** Hierarchical clustering of 289 differentially abundant (ANOVA significant) phosphorylation sites in control and DPI-treated (1h and 24 h 10 µM DPI) Be(2)-C cells. Each condition has 3 biological and 3 technical replicates. The values in the heatmap represent the Z-transformation of log2(LFQ intensity). Yellow represents high protein expression while blue represents low protein expression. Permutation-based FDR 0.01. **(B)** PCA analysis using a Benjamini-Hochberg FDR = 0.05. **(C)** Scatter plot, 1h DPI versus untreated control (Ctrl). A 3fold change (FC) was taken as cut-off. **(D)** The top 3 clusters out of 42 clusters following functional annotation clustering of up- and downregulated proteins using DAVID default annotation

categories. **(E)** Scatter plot, 24h DPI versus untreated control (Ctrl). A 3fold change (FC) was taken as cut-off. **(F)** The top 5 clusters out of 204 clusters following functional annotation clustering of up- and downregulated proteins using DAVID default annotation categories.

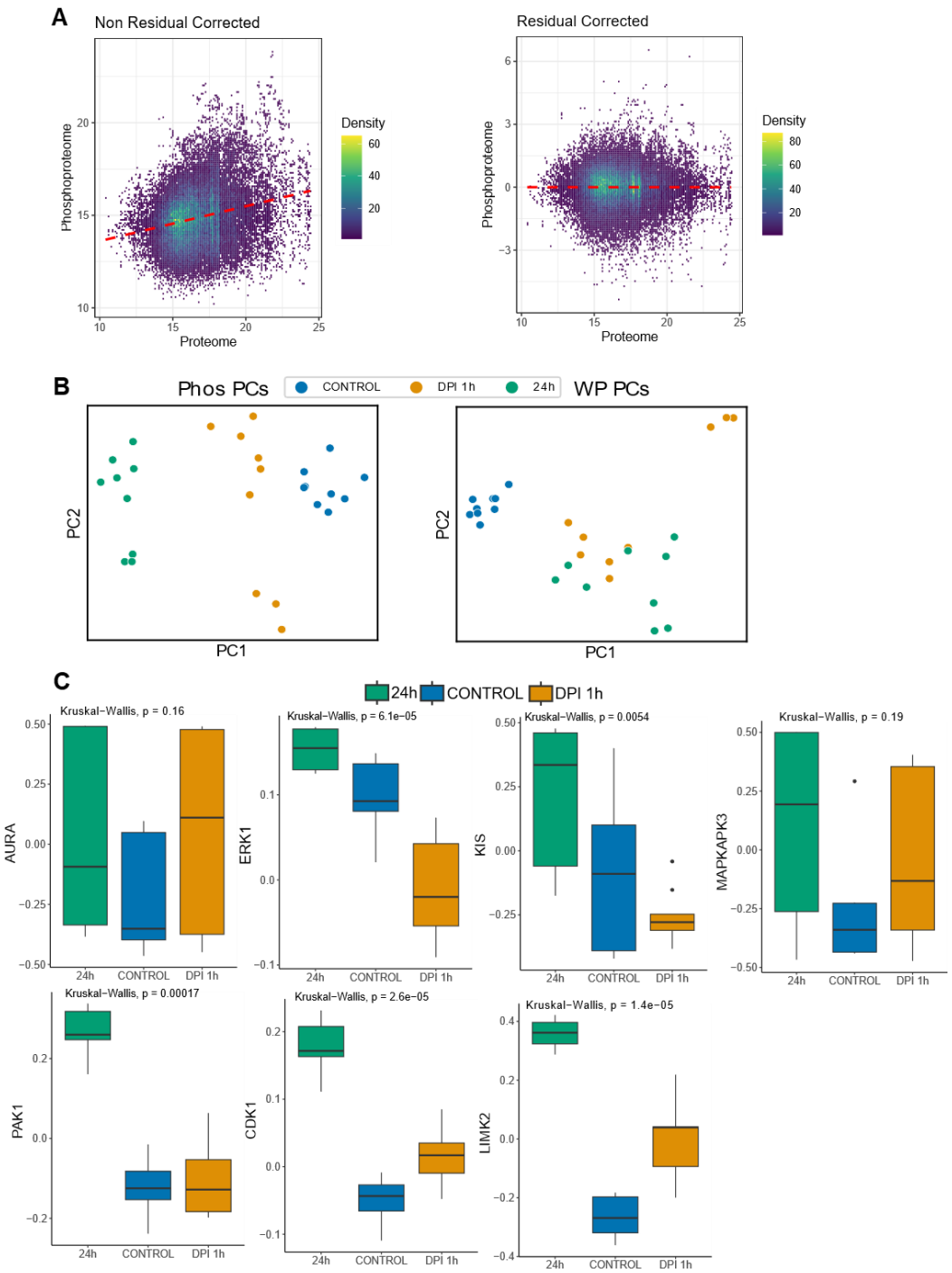

Supplementary Figure S3. Integration of total proteomics and phosphoproteomics data of DPI-treated Be(2)-C cells by multiset correlation and factor analysis. **(A)** The relationship between the expression of a protein and its phosphorylation sites. Left panel: pre-normalization of the phosphoproteomics by the whole proteomics data. Right panel: post-normalization of the phosphoproteomics by the whole proteomics data. **(B)** PCA analyses of data frames that represent the activity of pathways and kinases in each sample. **(C)** Kinase activity changes inferred by Kinase–Substrate Enrichment Analysis (KSEA).

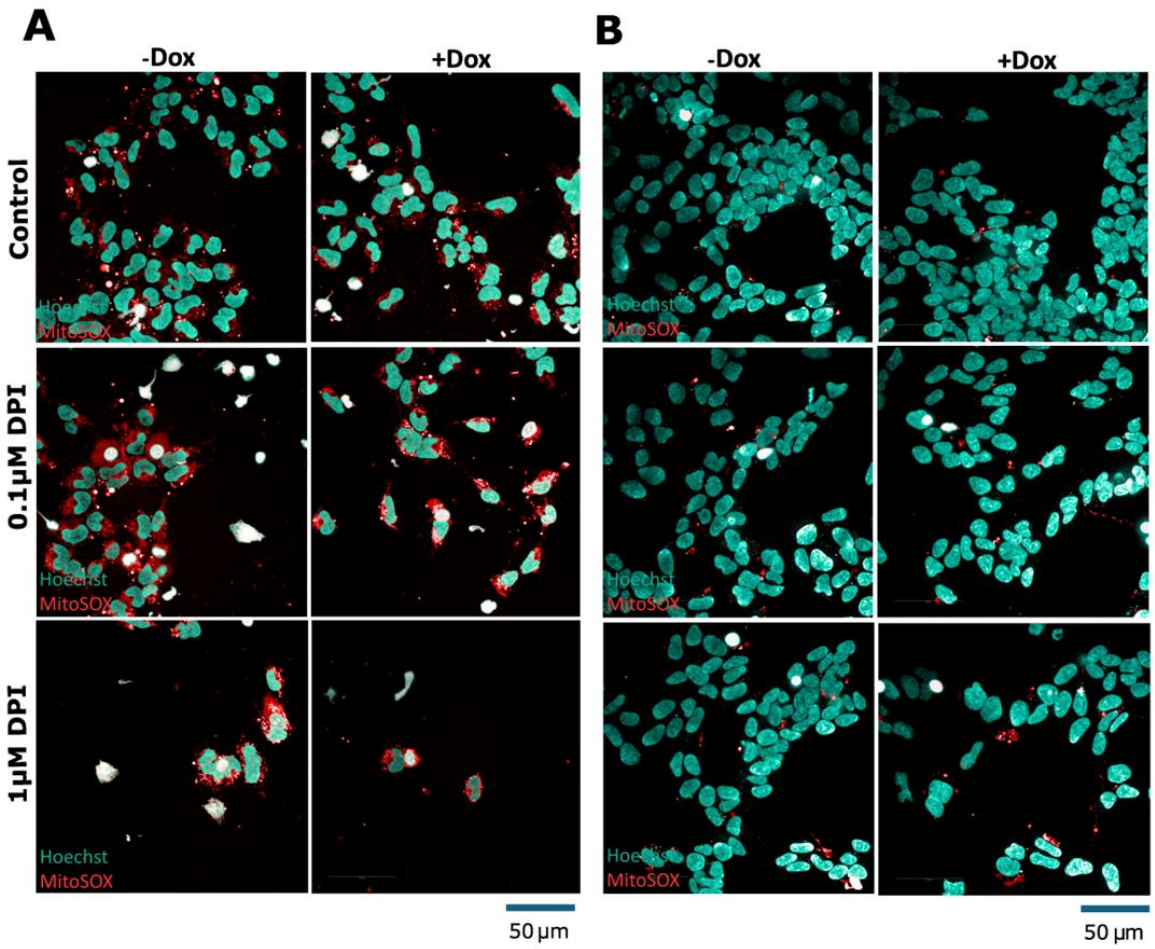

Supplementary Figure S4. DPI induces mitochondrial superoxide production dependent on MYCN levels. **(A)** Representative microscopic images of mitochondrial superoxide production detected by MitoSOX in SH-SY5Y/MYCN +/-Dox treated with DPI for 24 hours. Red, superoxide; green, nuclei. **(B)** Representative microscopic images of mitochondrial superoxide production detected by MitoSOX in IMR-5/75 +/-Dox treated with DPI for 24 hours. Red, superoxide; green, nuclei.

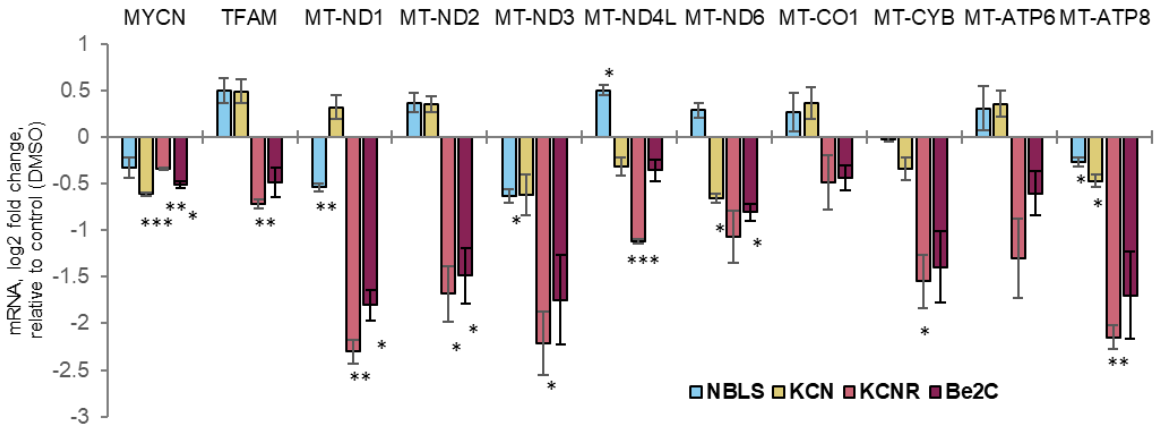

Supplementary Figure S5. DPI modulates the expression of mitochondrial genes and MYCN. The effect of DPI (1µM, 24 h) on mitochondrial gene expression and MYCN was assayed by RT-PCR. Data are shown as fold change over control (DMSO). (Mean ± SEM; N=3; ***$p < 0.001$, **$p < 0.01$ and *$p < 0.05$ DPI vs DMSO).

References

[1] Matthay, K., Maris, J., Schleiermacher, G. *et al.* Neuroblastoma. *Nat Rev Dis Primers* **2**, 16078 (2016).

[2] Friedman, D. N. & Henderson, T. O. Late Effects and Survivorship Issues in Patients with Neuroblastoma. *Children (Basel)* **5** (2018).

[3] Otte, J., Dyberg, C., Pepich, A. & Johnsen, J. I. MYCN Function in Neuroblastoma Development. *Front Oncol* **10**, 624079 (2020).

[4] Wolpaw, A. J. *et al.* Drugging the "Undruggable" MYCN Oncogenic Transcription Factor: Overcoming Previous Obstacles to Impact Childhood Cancers. *Cancer Res* **81**, 1627-1632 (2021).

[5] Epp, S., Chuah, S. M. & Halasz, M. Epigenetic Dysregulation in MYCN-Amplified Neuroblastoma. *Int J Mol Sci* **24** (2023).

[6] Ruiz-Pérez, M. V., Henley, A. B. & Arsenian-Henriksson, M. The MYCN Protein in Health and Disease. *Genes (Basel)* **8** (2017).

[7] Riganti, C. *et al.* Diphenyleneiodonium inhibits the cell redox metabolism and induces oxidative stress. *J Biol Chem* **279**, 47726-47731 (2004).

[8] Lambert, A. J., Buckingham, J. A., Boysen, H. M. & Brand, M. D. Diphenyleneiodonium acutely inhibits reactive oxygen species production by mitochondrial complex I during reverse, but not forward electron transport. *Biochim Biophys Acta* **1777**, 397-403 (2008).

[9] Alborzinia, H. *et al.* MYCN mediates cysteine addiction and sensitizes neuroblastoma to ferroptosis. *Nat Cancer* **3**, 471-485 (2022).

[10] Wang, T. *et al.* MYCN drives glutaminolysis in neuroblastoma and confers sensitivity to an ROS augmenting agent. *Cell Death Dis* **9**, 220 (2018).

[11] Brady, S. W. *et al.* Pan-neuroblastoma analysis reveals age- and signature-associated driver alterations. *Nat Commun* **11**, 5183 (2020).

[12] Duffy, D. J. *et al.* Integrative omics reveals MYCN as a global suppressor of cellular signalling and enables network-based therapeutic target discovery in neuroblastoma. *Oncotarget* **6**, 43182-43201 (2015).

[13] Svensson, A., Azarbayjani, F., Bäckman, U., Matsumoto, T. & Christofferson, R. Digoxin inhibits neuroblastoma tumor growth in mice. *Anticancer Res* **25**, 207-212 (2005).

[14] Russo, V. C., Metaxas, S., Kobayashi, K., Harris, M. & Werther, G. A. Antiapoptotic effects of leptin in human neuroblastoma cells. *Endocrinology* **145**, 4103-4112 (2004).

[15] Dzieran, J. *et al.* MYCN-amplified neuroblastoma maintains an aggressive and undifferentiated phenotype by deregulation of estrogen and NGF signaling. *Proc Natl Acad Sci U S A* **115**, E1229-e1238 (2018).

[16] Bierbrauer, A., Jacob, M., Vogler, M. & Fulda, S. A direct comparison of selective BH3-mimetics reveals BCL-X(L), BCL-2 and MCL-1 as promising therapeutic targets in neuroblastoma. *Br J Cancer* **122**, 1544-1551 (2020).

[17] Lamers, F. *et al.* Targeted BCL2 inhibition effectively inhibits neuroblastoma tumour growth. *Eur J Cancer* **48**, 3093-3103 (2012).

[18] Phimmachanh, M., Han, J. Z. R., O'Donnell, Y. E. I., Latham, S. L. & Croucher, D. R. Histone Deacetylases and Histone Deacetylase Inhibitors in Neuroblastoma. *Front Cell Dev Biol* **8**, 578770 (2020).

[19] Krstic, A. *et al.* A Chemo-Genomic Approach Identifies Diverse Epigenetic Therapeutic Vulnerabilities in MYCN-Amplified Neuroblastoma. *Front Cell Dev Biol* **9**, 612518 (2021).

[20] Hastings, J. F. *et al.* Memory of stochastic single-cell apoptotic signaling promotes chemoresistance in neuroblastoma. *Sci Adv* **9**, eabp8314 (2023).

[21] Messina, E. *et al.* Guanine nucleotide depletion triggers cell cycle arrest and apoptosis in human neuroblastoma cell lines. *Int J Cancer* **108**, 812-817 (2004).

[22] Moreno, L. *et al.* A phase I trial of AT9283 (a selective inhibitor of aurora kinases) in children and adolescents with solid tumors: a Cancer Research UK study. *Clin Cancer Res* **21**, 267-273 (2015).

[23] Fetahu, I. S. & Taschner-Mandl, S. Neuroblastoma and the epigenome. *Cancer and Metastasis Reviews* **40**, 173-189 (2021).

[24] Li, X. & Jiang, L. H. A critical role of the transient receptor potential melastatin 2 channel in a positive feedback mechanism for reactive oxygen species-induced delayed cell death. *J Cell Physiol* **234**, 3647-3660 (2019).

[25] Yamamuro-Tanabe, A., Oshima, Y., Iyama, T., Ishimaru, Y. & Yoshioka, Y. Proteasome inhibitors induce apoptosis by superoxide anion generation via NADPH oxidase 5 in human neuroblastoma SH-SY5Y cells. *J Pharmacol Sci* **155**, 52-62 (2024).

[26] Muth, D. *et al.* Transcriptional repression of SKP2 is impaired in MYCN-amplified neuroblastoma. *Cancer Res* **70**, 3791-3802 (2010).

[27] Brown, B.C., Wang, C., Kasela, S. *et al.* Multiset correlation and factor analysis enables exploration of multi-omics data, *Cell Genomics*, Volume 3, Issue 8, 2023, 100359.

[28] Nguyen, T. T. T. *et al.* Aurora kinase A inhibition reverses the Warburg effect and elicits unique metabolic vulnerabilities in glioblastoma. *Nat Commun* **12**, 5203 (2021).

[29] Prickaerts, P. *et al.* MK3 modulation affects BMI1-dependent and independent cell cycle check-points. *PLoS One* **10**, e0118840 (2015).

[30] Rosario, S. R. *et al.* Pan-cancer analysis of transcriptional metabolic dysregulation using The Cancer Genome Atlas. *Nat Commun* **9**, 5330 (2018).

[31] Belosludtseva, N. V., Matveeva, L. A. & Belosludtsev, K. N. Mitochondrial Dyshomeostasis as an Early Hallmark and a Therapeutic Target in Amyotrophic Lateral Sclerosis. *Int J Mol Sci* **24** (2023).

[32] Kim, J. E., Ryu, H. J., Kim, M. J. & Kang, T. C. LIM kinase-2 induces programmed necrotic neuronal death via dysfunction of DRP1-mediated mitochondrial fission. *Cell Death Differ* **21**, 1036-1049 (2014).

[33] Xie, B., Wang, S., Jiang, N. & Li, J. J. Cyclin B1/CDK1-regulated mitochondrial bioenergetics in cell cycle progression and tumor resistance. *Cancer Lett* **443**, 56-66 (2019).

[343] Ahn, M. *et al.* A requirement for PAK1 to support mitochondrial function and maintain cellular redox balance via electron transport chain proteins to prevent β-cell apoptosis. *Metabolism* **115**, 154431 (2021).

[35] Nolfi-Donegan, D., Braganza, A. & Shiva, S. Mitochondrial electron transport chain: Oxidative phosphorylation, oxidant production, and methods of measurement. *Redox Biol* **37**, 101674 (2020).

[36] Doroshow, J. H., Esworthy, R. S. & Chu, F. F. Control of doxorubicin-induced, reactive oxygen-related apoptosis by glutathione peroxidase 1 in cardiac fibroblasts. *Biochem Biophys Rep* **21**, 100709 (2020).

[37] Garrido, C. *et al.* Mechanisms of cytochrome c release from mitochondria. *Cell Death Differ* **13**, 1423-1433 (2006).

[38] Morrish, F., Giedt, C. & Hockenbery, D. c-MYC apoptotic function is mediated by NRF-1 target genes. *Genes Dev* **17**, 240-255 (2003).

[39] Hanahan, D. Hallmarks of Cancer: New Dimensions. *Cancer Discov* **12**, 31-46 (2022).

[40] Franken, N. A., Rodermond, H. M., Stap, J., Haveman, J. & van Bree, C. Clonogenic assay of cells in vitro. *Nat Protoc* **1**, 2315-2319 (2006).

[41] Qin, X. *et al.* CKLF instigates a "cold" microenvironment to promote MYCN-mediated tumor aggressiveness. *Sci Adv* **10**, eadh9547 (2024).

[42] Anderson, N. M. *et al.* Metabolic Enzyme DLST Promotes Tumor Aggression and Reveals a Vulnerability to OXPHOS Inhibition in High-Risk Neuroblastoma. *Cancer Res* **81**, 4417-4430 (2021).

[43] Zhu, S. *et al.* LMO1 Synergizes with MYCN to Promote Neuroblastoma Initiation and Metastasis. *Cancer Cell* **32**, 310-323.e315 (2017).

[44] Tao, T. *et al.* The pre-rRNA processing factor DEF is rate limiting for the pathogenesis of MYCN-driven neuroblastoma. *Oncogene* **36**, 3852-3867 (2017).

[45] Zhu, S. *et al.* Activated ALK collaborates with MYCN in neuroblastoma pathogenesis. *Cancer Cell* **21**, 362-373 (2012).

[46] Aldieri, E. *et al.* Classical inhibitors of NOX NAD(P)H oxidases are not specific. *Curr Drug Metab* **9**, 686-696 (2008).

[47] Gustafson, W. C. *et al.* Drugging MYCN through an allosteric transition in Aurora kinase A. *Cancer Cell* **26**, 414-427 (2014).

[48] Mossé, Y. P. *et al.* A Phase II Study of Alisertib in Children with Recurrent/Refractory Solid Tumors or Leukemia: Children's Oncology Group Phase I and Pilot Consortium (ADVL0921). *Clin Cancer Res* **25**, 3229-3238 (2019).

[49] Roeschert, I. *et al.* Combined inhibition of Aurora-A and ATR kinase results in regression of MYCN-amplified neuroblastoma. *Nat Cancer* **2**, 312-326 (2021).

[50] Liu, Z., Chen, S. S., Clarke, S., Veschi, V. & Thiele, C. J. Targeting MYCN in Pediatric and Adult Cancers. *Front Oncol* **10**, 623679 (2020).

[51] Wasylishen, A. R. *et al.* MYC phosphorylation at novel regulatory regions suppresses transforming activity. *Cancer Res* **73**, 6504-6515 (2013).

[52] Oliynyk, G. *et al.* MYCN-enhanced Oxidative and Glycolytic Metabolism Reveals Vulnerabilities for Targeting Neuroblastoma. *iScience* **21**, 188-204 (2019).

[53] Mukherjee, S., Bhatti, G. K., Chhabra, R., Reddy, P. H. & Bhatti, J. S. Targeting mitochondria as a potential therapeutic strategy against chemoresistance in cancer. *Biomed Pharmacother* **160**, 114398 (2023).

[54] Epp, S. *et al.* OXPHOS TARGETING OF MYCN-AMPLIFIED NEUROBLASTOMA. *bioRxiv*, 2024.2008.2003.606365 (2024).

[55] Schneider, C., Rasband, W. & Eliceiri, K. NIH Image to ImageJ: 25 years of image analysis. *Nat Methods* **9**, 671–675 (2012).

[56] Halasz M. *et al.* Integrating network reconstruction with mechanistic modeling to predict cancer therapies. *Sci. Signal*. **9**, ra114-ra114 (2016).

[57] Stefka, T., Temu, T., Sinitcyn, P. *et al.* The Perseus Computational Platform for Comprehensive Analysis of (Prote)omics Data. *Nature Methods* **13** (9): 731–40. (2016)

[58] Sherman, T., Hao, M., Qiu, J. *et al.* DAVID: a web server for functional enrichment analysis and functional annotation of gene lists (2021 update). *Nucleic Acids Research*. (2022).

[59] Kim, H. J., Kim, T., Hoffman, N.J. *et al.* PhosR enables processing and functional analysis of phosphoproteomic data. *Cell Reports* **34**(8) 108771 (2021).